Infrared Spectra and DFT Calculations for the Coinage Metal Hydrides MH, $(H_2)MH$, MH_2, M_2H, M_2H^-, and $(H_2)CuHCu$ in Solid Argon, Neon, and Hydrogen

Xuefeng Wang and Lester Andrews*

Department of Chemistry, University of Virginia, Charlottesville, Virginia 22904-4319

Laurent Manceron

LADIR/Spectrochimie Moléculaire CNRS UMR 7075, Université Pierre et Marie Curie, case 49, 4 place Jussieu 75252 Paris, France

Colin Marsden

Laboratoire de Physique Quantique, UMR 5626, IRSAMC, Université Paul Sabatier, 118 Route de Narbonne, 31062 Toulouse Cedex 4, France

Received: May 23, 2003; In Final Form: July 30, 2003

Laser-ablated coinage metal atom reactions with H_2 in excess argon, neon, and pure hydrogen are investigated through matrix infrared spectroscopy. The reaction products are identified by isotopic substitution (D_2, HD, and $H_2 + D_2$) and verified by DFT calculations of vibrational fundamentals. The MH and $(H_2)MH$ molecules are observed for all group 11 metals, and the trihydride complex $(H_2)AuH_3$ is stabilized in pure hydrogen. The $(H_2)CuH$ and $(H_2)AgH$ complexes exhibit weak H−H stretching fundamentals at 3805.9 and 3566.6 cm^{-1} and strong Cu−H and Ag−H stretching modes at 1861.4 and 1742.6 cm^{-1}, respectively. In addition, $(H_2)CuH$ reacts further with Cu to give $(H_2)CuHCu$, and Au (^2P) inserts to form AuH_2 in pure hydrogen. The cluster hydrides M_2H and M_2H^- anions are also formed in these experiments.

Introduction

The coinage metal hydrides have been intensively studied for many years both experimentally and theoretically because the activation of molecular hydrogen by late transition metals is important to understanding heterogeneous catalysis. Although copper hydride forms a stable solid-state compound,[1a] the absorption spectrum of CuH has been tentatively identified in sunspots and carbon stars.[1b] The CuH and CuD diatomic molecules have been observed in a copper hollow cathode lamp in a flow of H_2/Ne or D_2/Ne, vibration−rotation emission spectra of CuH have been recorded, and the Cu−H stretching fundamental vibration measured as 1866.4 cm^{-1}.[2a] All of the diatomic coinage metal hydrides and deuterides have been detected by vibration−rotation emission spectroscopy using a carbon-tube furnace.[2b] The infrared absorption of CuH has also been observed in low-temperature matrices through hollow-cathode discharge in argon and irradiation of reagents in krypton.[3] The $A^1\Sigma^+ \rightarrow X^1\Sigma^+$ emission of AgH in the region 21 250−33 300 cm^{-1} was investigated in 1931,[4] and the results are summarized by Huber and Herzberg.[5] The $A^1\Sigma^+$ state was found to be strongly perturbed by higher excited states.[6] However, there has been no low-temperature matrix work done for silver hydrides to the best of our knowledge. Recently, gold hydrides were investigated using laser-ablated atomic Au as a reagent, and the metal hydrides and hydrogen complexes AuH, $(H_2)AuH$, and $(H_2)AuH_3$ have been observed in excess argon, neon, and pure deuterium.[7]

Computational investigations of coinage metal hydrides have been done, in part, because these molecules serve as prototype systems for relativistic effects. Various theoretical methods have been employed to study the ground-state properties and comparisons of spectroscopic parameters were given to understand the bonding and perturbation of electronic states.[8]

In this paper, we present a matrix infrared investigation of laser-ablated copper and silver atom reactions with hydrogen in argon, neon, pure H_2, D_2, and HD matrices. The structures, vibrational frequencies, and infrared intensities of metal hydrides and complexes are confirmed by isotopic substitution and DFT calculations. The reactions of laser-ablated gold and hydrogen in pure H_2, $H_2 + D_2$, and HD are also included for comparison.

Experimental and Computational Methods

The experiments for reactions of laser-ablated copper, silver, and gold atoms with small molecules during condensation in excess argon and neon have been described in detail previously.[9] The Nd:YAG laser fundamental (1064 nm, 10 Hz repetition rate with 10 ns pulse width) was focused onto rotating metal targets (Johnson Matthey), and the laser energy was varied from 10 to 20 mJ/pulse. Laser-ablated metal atoms were co-deposited with hydrogen (1 to 5%) in excess argon, neon or pure hydrogen onto a 3.5 K CsI window at 5−3 mmol/hour for 60 or 30 min. Hydrogen, deuterium (Matheson), HD (Cambridge Isotopic Laboratories), and selected mixtures were used in different experiments. FTIR spectra were recorded at 0.5 cm^{-1} resolution on Nicolet 750 with 0.1 cm^{-1} accuracy using an HgCdTe detector. Matrix samples were annealed at different temperatures and subjected to broadband photolysis by a medium-pressure mercury arc lamp (Philips, 175W) with the globe removed.

DFT (density functional theory) calculations of metal hydrides and hydrogen complexes are given for comparison. The Gauss-

* Corresponding author. E-mail: lsa@virginia.edu.

10.1021/jp0354346 CCC: $25.00
Published on Web 09/13/2003

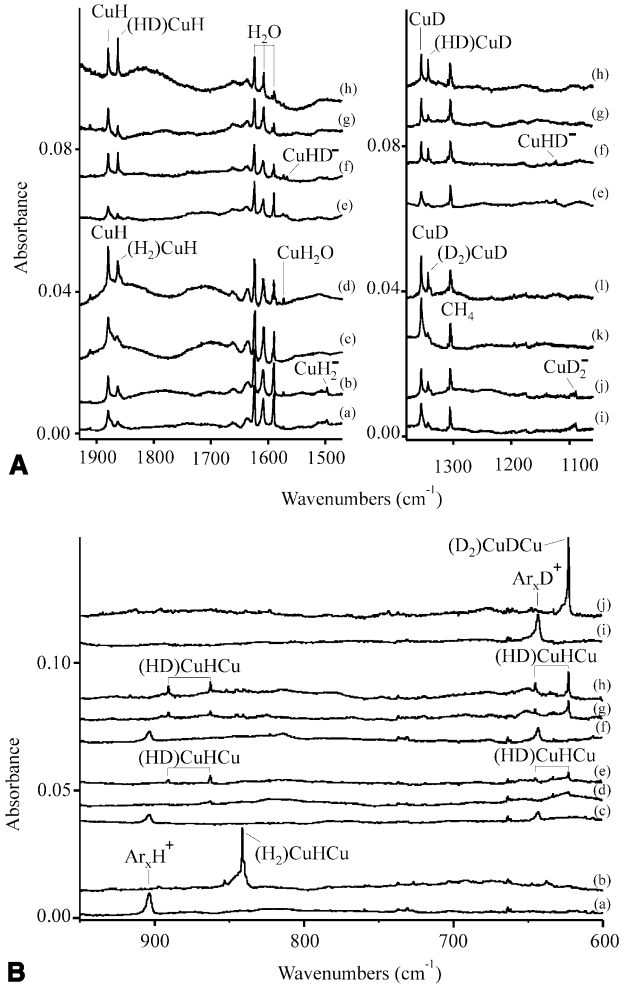

Figure 1. A. Infrared spectra in the 1930−1470 and 1380−1060 cm^{-1} regions for laser-ablated copper co-deposited with isotopic dihydrogen molecules in excess argon at 3.5 K for 60 min periods: (a) for 5% H_2; (b) after annealing to 15 K; (c) after λ > 240 nm photolysis for 15 min; (d) after annealing to 20 K; (e) for 5% HD; (f) after annealing to 19 K; (g) after λ > 240 nm photolysis for 15 min; (h) after annealing to 19 K; (i) for 5% D_2; (j) after annealing to 15 K; (k) after λ > 240 nm photolysis for 15 min; (l) after annealing to 20 K. B. Infrared spectra in the 920−600 cm^{-1} region for laser-ablated copper co-deposited with isotopic dihydrogen molecules in excess argon at 3.5 K for 60 min periods: (a) for 5% H_2; (b) after annealing to 15 K; (c) for 4% H_2 + 4% D_2; (d) after annealing to 15 K; (e) for 5% HD; (f) after annealing to 19 K; (g) for 5% D_2; (h) after annealing to 15 K.

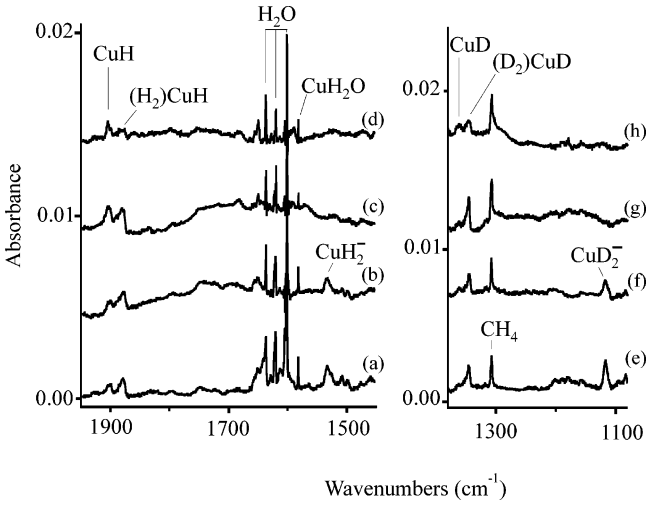

Figure 2. Infrared spectra in the 1950−1450 and 1380−1080 cm^{-1} regions for laser-ablated copper co-deposited with isotopic dihydrogen molecules in excess neon at 3.5 K for 60 min periods: (a) for 5% H_2; (b) after annealing to 6 K; (c) after λ > 240 nm photolysis; (d) after annealing to 11 K; (e) for 5% D_2; (f) after annealing to 6 K; (g) after λ > 240 nm photolysis; (h) after annealing to 11 K.

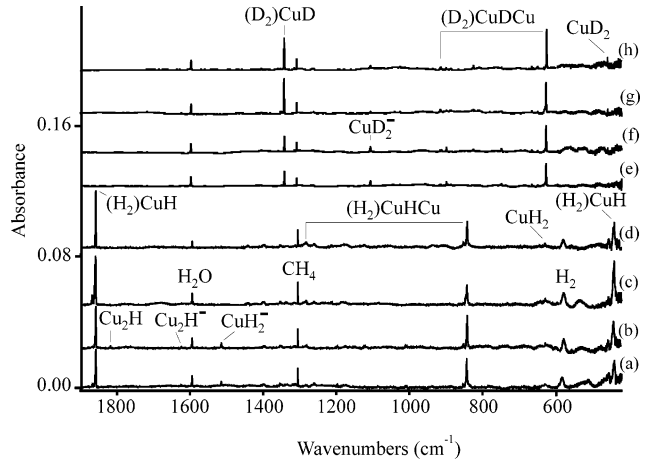

Figure 3. Infrared spectra in the 1900−420 cm^{-1} region for laser-ablated copper reaction products in pure normal hydrogen and deuterium at 3.5 K: (a) after co-deposition of Cu and pure H_2 for 25 min; (b) after annealing to 6.0 K; (c) after λ > 240 nm photolysis; (d) after annealing to 6.5 K; (e) after co-deposition of Cu and pure D_2 for 25 min; (f) after annealing to 7.0 K; (g) after λ > 240 nm photolysis; (h) after annealing to 8.0 K.

ian 98 program[10] was employed to calculate the structures and frequencies of expected molecules. The 6-311++G(d,p) basis set for H and SDD and LANL2DZ pseudopotentials for copper, silver, and gold atoms were used.[11] All geometrical parameters were fully optimized with the BPW91 and B3LYP functionals.[12,13] The BPW91 functional has been recommended for coinage-metal compounds.[8e] Analytical vibrational frequencies were obtained at the optimized structures.

Results

Infrared spectra of reaction products recorded in argon, neon, and pure H_2, D_2, and HD at 4 K are presented, and DFT calculations are used to support the product identifications from vibrational frequencies.

Cu + H_2. Infrared spectra in the Cu−H and Cu−D stretching regions are shown in Figures 1−3 for laser-ablated Cu atom reactions with H_2 in excess argon, neon and pure H_2 and D_2. In solid argon a strong band at 1879.8 cm^{-1} and a weak band at 1862.5 cm^{-1} were observed on deposition, and the weak band was enhanced on annealing, but reduced by full-arc photolysis in favor of the strong band. Further annealing to 30 K increased the 1862.5 cm^{-1} band and decreased the 1879.8 cm^{-1} band (Figure 1). Deuterium counterparts appeared at 1354.9 and 1343.2 cm^{-1}, respectively. On annealing to 20 K a sharp band at 841.2 cm^{-1} was produced, which shifts to 622.9 cm^{-1} with deuterium substitution. The absorptions due to A_nH^+ and Ar_nD^+ were observed in all argon matrix experiments.[14] Weaker photosensitive absorptions at 1497.2 and 1089.4 cm^{-1}, identified as CuH_2^- and CuD_2^- in Figure 1 and Table 1, will be discussed fully in another report.[15] The weak 1572.8 cm^{-1} band is in agreement with the previous assignment to a Cu(H_2O) complex, which gives way to a weak 1911 cm^{-1} (HCuOH) band on photolysis.[16] This band is observed at 1577.2 cm^{-1} in solid neon (Figure 2).

The Cu−H stretching frequencies in excess neon show reverse intensity features: two bands appeared at 1889.9 and

TABLE 1: Infrared Absorptions (cm^{-1}) Observed from Reactions of Copper Atoms and Dihydrogen in Excess Argon, Neon, and Hydrogen

argon			neon			hydrogen			
H_2	HD	D_2	H_2	HD	D_2	H_2	HD	D_2	identification
						3566.6			$(H_2)CuH$
								2582.0	$(D_2)CuD$
								2208.7	$(D_2)CuDCu$
			1894.4	1894.4					CuH (site)
1879.8	1879.8		1889.9	1889.9					CuH
	1354.9	1354.9		1362.2	1362.2				CuD
1862.5	1862.7		1869.1	1869.1		1861.4	1865.5		$(H_2)CuH$
	1343.0	1343.2		1346.4	1344.9		1345.4	1341.6	$(D_2)CuD$
						1821			Cu_2H
						1627.1	1630		$CuCuH^-$
								1194.8	$CuCuD^-$
1497.2	1497.2		1529.5			1517.8			CuH_2^-
	1566.9						1586.7		$CuHD^-$
	1122.7						1137.6		$CuHD^-$
	1089.4	1089.4			1116.5			1107.3	CuD_2^-
1270.8						1284.3			$(H_2)CuHCu$
		912.8						913.7	$(D_2)CuDCu$
841.2	890.6		847.3	847.3		845.3	885.6		$(H_2)CuHCu$
	862.5						844.8		(HD)CuHCu
	645.2			657.6			655.4		(HD)CuDCu
	622.9	622.9		628.2	628.2		627.3	626.2	$(D_2)CuDCu$
637.5									Cu_2H_y
						636.5			CuH_2
						441	424		$(H_2)CuH$
							573.1		CuHD
								458.5	CuD_2

1869.1 cm^{-1} on deposition, but the latter is much stronger than the former, indicating that the 1869.1 cm^{-1} band is favored by more diffusion in the neon matrix (Figure 2). The analogous Cu−D stretching frequencies are listed in Table 1.

In pure H_2, one strong band was observed in the upper region at 1861.4 cm^{-1} with an associated weaker absorption at 3566.6 cm^{-1}, which shift to 2582.0 and 1341.6 cm^{-1} in pure D_2, and a lower associated band is found in H_2 at 441 cm^{-1}. In addition, ultraviolet irradiation increased a new band at 636.5 cm^{-1} with D_2 counterpart at 458.5 cm^{-1} (Figure 3). With $H_2 + D_2$ broad bands are centered at 1863 and 1343 cm^{-1}, but pure HD gave sharp counterparts at 1865.5 and 1345.4 cm^{-1} along with a weak 573.1 cm^{-1} band. A 844.9 cm^{-1} band in pure H_2 and a 626.2 cm^{-1} band in pure D_2 appeared on deposition and increased on sequential annealing in the lower region.

Ag + H_2. Laser-ablated silver atom reactions with H_2 in excess argon at 3.5 K gave a weak band at 1717.0 cm^{-1}, which decreased on annealing to 20 K, and a weak absorption at 1735.8 cm^{-1}, which increased on annealing to 20 K, while a new band was produced at 1746.5 cm^{-1}. With full-arc photolysis the 1746.5 cm^{-1} band decreased and the 1717.0 cm^{-1} band increased, but this reversed on subsequent annealing to 30 K (Figure 4). A new band appeared at 1691.9 cm^{-1} on annealing to 30 K. The deuterium counterparts for these bands were found at 1233.8, 1247.2, 1257.6, and 1216.3 cm^{-1}. Similar absorptions were observed in neon matrix experiments (Table 2).

Pure H_2 and D_2 experiments gave more impressive results, which are compared in Figure 5. New bands are observed at 3805.9, 1742.6, 1691.5, 1523, and 1442.4 cm^{-1} in pure hydrogen. Photolysis ($\lambda > 290$ nm) destroyed the 1523 cm^{-1} peak, increased the 1442.4 cm^{-1} band by 20% and doubled the 1691.5 cm^{-1} absorption (not shown). The former two bands increased and the latter absorptions disappeared on full arc photolysis. A weak 2736.3 cm^{-1} band increased with the strong 1255.7 cm^{-1} absorption on 240 nm photolysis in pure deuterium whereas the 1045.9 cm^{-1} band decreased and the weak 1101.0 cm^{-1} absorption disappeared. The 1442.4 and 1045.9 cm^{-1} bands, identified as AgH_2^- and AgD_2^- in Table 2, will be considered in a separate paper.[15] Pure HD gave two strong absorptions at 1748.6 and 1255.4 cm^{-1}.

Au + H_2. Gold atoms were co-deposited with pure hydrogen, now technically possible in our laboratory, to compare with previous deuterium experiments.[7] Although the product yield was less using necessarily lower laser energy, several important absorptions were observed as listed in Table 3 and shown in Figure 6. New 2164.0 and 1661.5 cm^{-1} bands are counterparts to the pure deuterium product bands at 1556.5 and 1198.6 cm^{-1}. In addition, new 1283.2, 638.1, and 576.0 cm^{-1} bands are

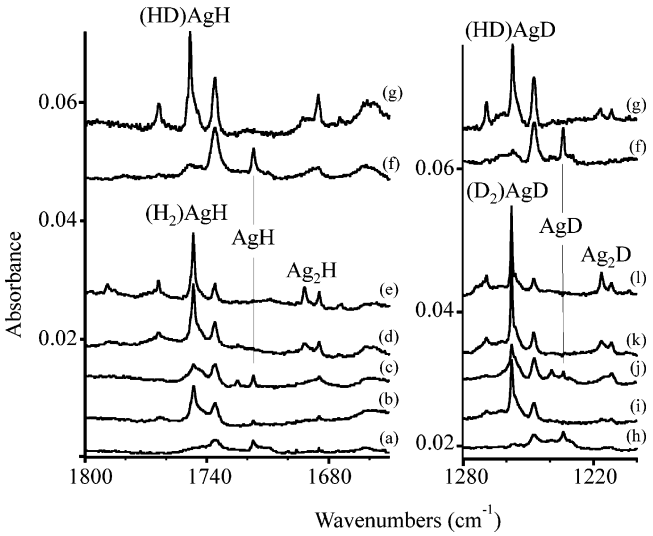

Figure 4. Infrared spectra for laser-ablated silver reaction products with isotopic hydrogen in excess argon at 3.5 K: (a) for 5% H_2 in argon co-deposited for 60 min; (b) after annealing to 20 K; (c) after $\lambda > 240$ nm photolysis; (d) after annealing to 25 K; (e) for 4% HD in argon; (f) after annealing, photolysis, and annealing to 25 K; (g) for 5% D_2 in argon; (h) after annealing to 20 K; (i) after $\lambda > 240$ nm photolysis; (j) after annealing to 25 K.

TABLE 2: Infrared Absorptions (cm^{-1}) Observed from Reactions of Silver Atoms and Dihydrogen in Excess Argon, Neon, and Hydrogen

argon			neon		hydrogen			
H_2	HD	D_2	H_2	D_2	H_2	HD	D_2	identification
					3805.9			$(H_2)AgH$
						3367.1		(HD)AgH, (HD)AgD
							2736.3	$(D_2)AgD$
1764.0		1269.2	1767.7					$(H_2)AgH$ site
1746.5	1748.2		1750.8		1742.6	1748.6		$(H_2)AgH$
	1256.9	1257.6		1264.3		1255.4	1255.7	$(D_2)AgD$
1735.8	1735.8							$(H_2)AgH$ site
	1247.4	1247.2						$(D_2)AgD$ site
1717.0	1717.0				1692			AgH
	1233.8	1233.8						AgD
1691.9	1691.9		1699		1692			AgAgH
	1216.3	1216.3		1222			1218	AgAgD
1684.8								Ag_xH
		1211.8						Ag_xD
-			1516		1523	1523		$AgAgH^-$
				1097			1101	$AgAgD^-$
1427.5	1427.5		1460		1442.4			AgH_2^-
	1496.8							$AgHD^-$
	1068.9							$AgHD^-$
	1032.3	1032.3		1053			1045.9	AgD_2^-
			1324.1		1320.9			$AgHAg^-$
				957.3			955.9	$AgDAg^-$

TABLE 3: Infrared Absorptions (cm^{-1}) Observed from Reactions of Gold Atoms with Pure Dihydrogen Isotopic Molecules

H_2	HD	$H_2 + D_2$	D_2	identification
	3026.0, 3022.3			(HD)AuH, (HD)AuD
2164.0	2162.7	2163.6, 2156.5		$(H_2)AuH$, (HD)AuH, $(D_2)AuH$
	1555.2	1560.9, 1555.7	1556.5	(HD)AuD, $(H_2)AuD$, $(D_2)AuD$
2082				AuAuH
			1493	AuAuD
1991.7	1991.7			$AuAuH^-$
	1434.5		1434.5	$AuAuD^-$
1678.8				AuH_4^- site
1676.4				AuH_4^-
1666.8				$(H_2)AuH_3$ site
			1205.9	$(D_2)AuD_3$ site
1661.5	1821.4	1663.7		$(H_2)AuH_3$
	1267.1	1197.0	1198.6	$(D_2)AuD_3$
	1840.4	1681.3		$AuH_2D_2^-$
	1280.4	1211.3		$AuH_2D_2^-$
			1213.6	AuD_4^- site
			1212.2	AuD_4^-
1636.0				AuH_2^-
			1182.3	AuD_2^-
1283.2				$(H_2)AuH$
			939.6	$(D_2)AuD$
638.2				AuH_2
	570.6			AuHD
			457.0	AuD_2
576.0				$(H_2)AuH$
			434.8	$(D_2)AuD$

counterpart to deuterium product bands at 939.6, 457.0, and 434.8 cm^{-1}. The weaker 1676.4 cm^{-1} and deuterium counterpart 1212.2 cm^{-1} bands will be identified as AuH_4^- and AuD_4^- anions in a subsequent report.[15] A pure $H_2 + D_2$ experiment gave slightly shifted doublets at 2163.7, 2156.6 cm^{-1} and at 1561.0, 1556.3 cm^{-1} with relative band areas of 5/1 and weaker bands at 1663.8 and 1197.9 cm^{-1} with relative band areas of 3/1. Finally, related absorptions were also observed with pure HD at 2162.7 and 1555.2 cm^{-1} and at 1821.4 and 1267.1 cm^{-1}, which are illustrated in Figure 6 and listed in Table 3. In addition, new 3026.0, 3022.3 cm^{-1} and very weak bands were observed at 1660.5 and 1195.4 cm^{-1}: A weak 570.6 cm^{-1} band increased on 240 nm photolysis and on 7.0 K annealing.

Complementary hydrogen matrix experiments were performed with ultraviolet photolysis of thermal gold atoms on a copper surface cooled to about 3 K by a cryogenerator (Cryomech PT405).[17,18] Normal hydrogen (deuterium) (3 mmol) was co-deposited for 30 min with thermal gold atoms monitored by a microbalance. The first hydrogen experiment, owing to the less efficient condensation of H_2 (FP 14.0 K) resulted in a dark brown sample; however, no Au_3 was detected in the vibronic transition near 2000 cm^{-1}.[19] A very weak 2164.2 cm^{-1} absorption was observed on sample deposition: This band increased markedly on 265 nm photolysis and 1314.6, 638.1, and 575.8 cm^{-1} bands appeared. Annealing to 6.0 K produced no changes in the spectrum, and annealing to 6.5 K allowed the H_2 sample to evaporate. The next deposition employed deuterium at the same rates, but the more efficient condensation of D_2 (FP 18.6 K) gave a clear tan sample. Photolysis at 265 nm produced strong new bands at 1556.6, 457.0, and 434.5 cm^{-1}

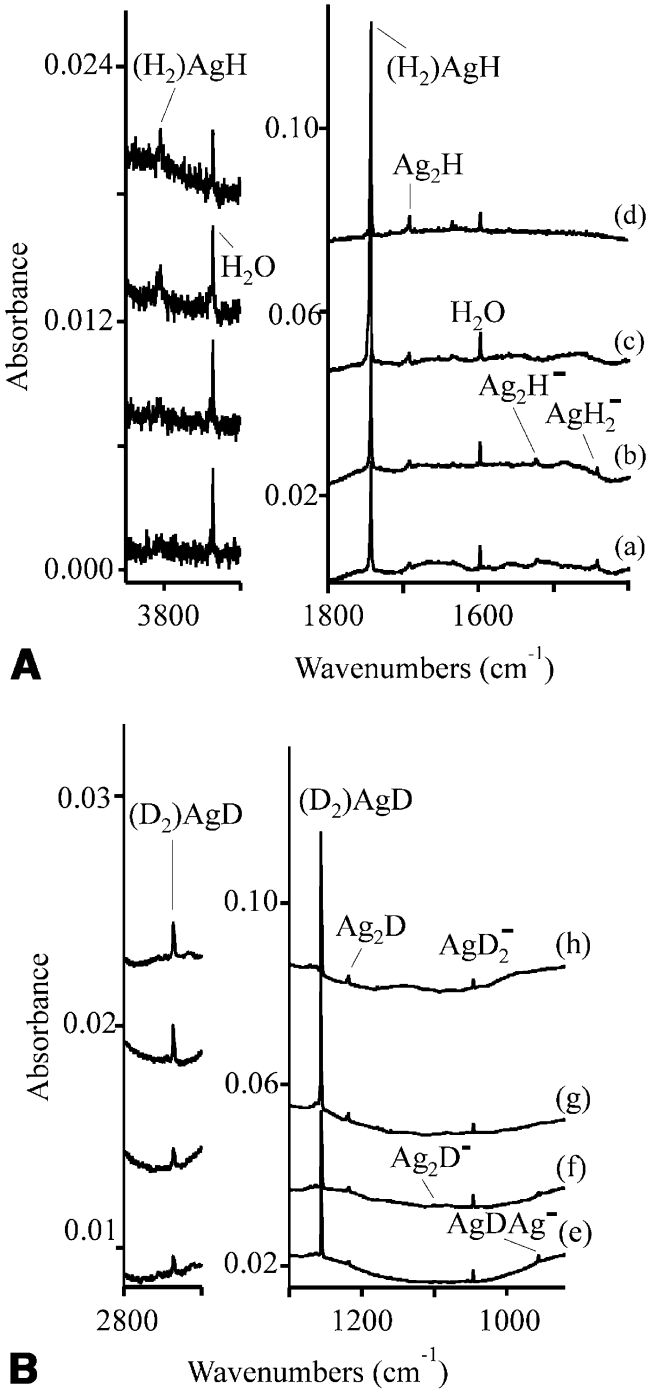

Figure 5. A. Infrared spectra in the 3850−3700 and 1800−1400 cm^{-1} regions for laser ablated silver co-deposited with pure hydrogen at 3.5 K: (a) after co-deposition of Ag and pure H_2 for 25 min; (b) after annealing to 6.0 K; (c) after $\lambda > 240$ nm photolysis; (d) after annealing to 6.6 K. B. Infrared spectra in the 2800−2700 and 1300−920 cm^{-1} regions for laser ablated silver co-deposited with pure deuterium at 3.5 K: (a) after co-deposition of Ag and pure H_2 for 25 min; (b) after annealing to 6.0 K; (c) after $\lambda > 240$ nm photolysis; (d) after annealing to 6.6 K; (e) after co-deposition of Ag and pure H_2 for 25 min; (f) after annealing to 6.5 K; (g) after $\lambda > 240$ nm photolysis; (h) after annealing to 7.5 K.

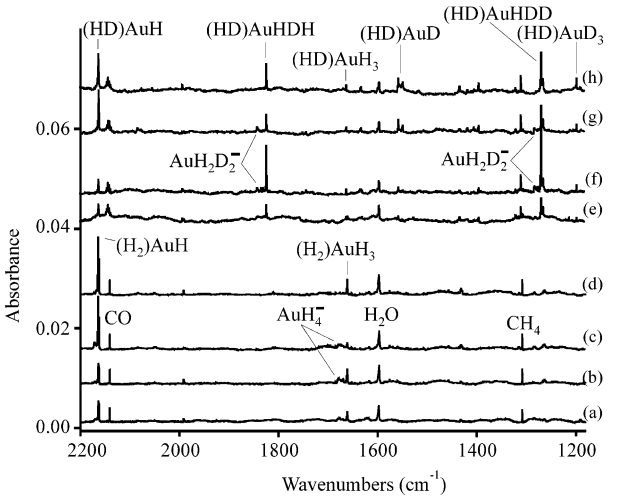

Figure 6. Infrared spectra in the 2200−1180 cm^{-1} region for laser ablated gold co-deposited with pure H_2 and with pure HD at 3.5 K: (a) for Au and pure H_2; (b) after $\lambda > 290$ nm photolysis; (c) after $\lambda > 240$ nm photolysis; (d) after annealing to 6.0 K; (e) for Au + pure HD; (f) after $\lambda > 290$ nm photolysis; (g) after $\lambda > 240$ nm photolysis; and (h) after annealing to 7.0 K.

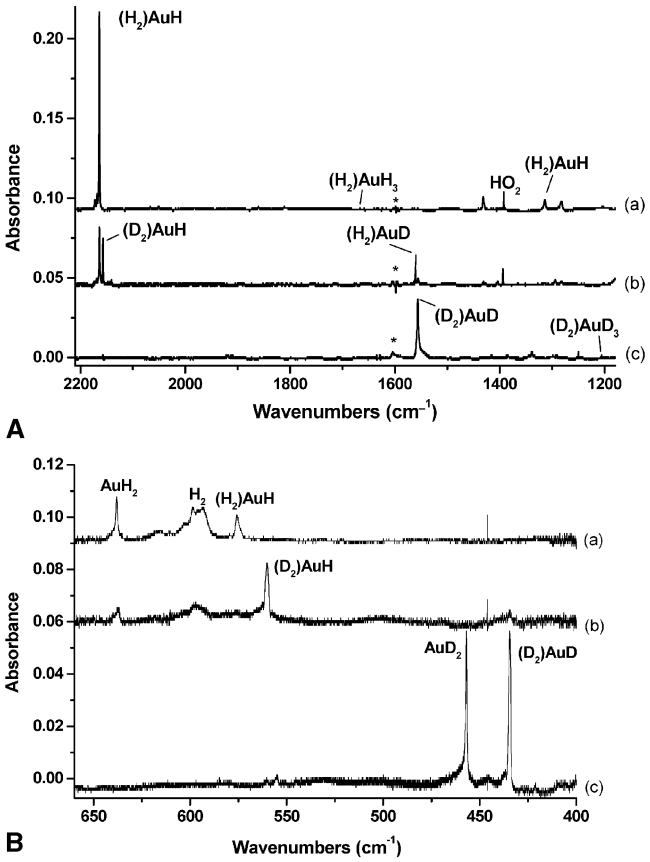

Figure 7. A. Infrared spectra in the 2200−1180 cm^{-1} region for thermally evaporated gold co-deposited with hydrogen on a copper surface near 3 K. Plotted spectra are difference spectrum after 265 nm dielectric spike filter resonance photolysis minus spectrum of deposited sample before photolysis. The ∗ denotes H_2O. Spectra recorded at 0.1 cm^{-1} resolution on MCTA detector for (a) H_2, (b) $H_2 + D_2$, and (c) D_2. B. Infrared spectra in the 650−400 cm^{-1} region for samples described in Figure 7A caption. Spectra recorded at 0.1 cm^{-1} resolution on a bolometer detector for (a) H_2, (b) $H_2 + D_2$, and (c) D_2.

and a weak new band at 1205.9 cm^{-1} ($A = 0.003$), which are illustrated in Figure 7, parts A and B, as the difference between after and before photolysis. Another weak band at 939.6 cm^{-1} ($A = 0.025$) is not shown.

Another hydrogen experiment with 50% as much gold gave a clear tan sample: 265 nm photolysis produced the strong 2164.2 cm^{-1}, medium 1314.6, 638.1, and 575.8 cm^{-1}, and very weak 1666.8 cm^{-1} ($A = 0.001$) absorptions shown in Figure 7A. A final experiment with 50% H_2 + 50% D_2 and the lower

gold deposition produced more absorptions: The middle spectra show the 2163.9, 2156.8, 1561.0, 1566.0 cm^{-1} quartet and new 637.4, 575.2, 560.2, and 434.4 cm^{-1} absorptions. The two higher bands in the quartet are five times stronger than the two lower bands. In these more dilute gold experiments the Au/H_2 ratio is estimated to be about 1/1000.

Calculations. DFT calculations were done for copper hydrides using two functionals, and the SDD pseudopotential for copper, and the results are summarized in Table 4. All-electron calculations for the smaller copper hydrides using the 6-311++G(d,p) basis sets gave similar results. The ground state of CuH is predicted to be $^1\Sigma^+$ with 1.477 Å bond length and 1909.1 cm^{-1} harmonic frequency at the BPW91/6-311++G(d,p) level of theory. This calculation is very close to the latest gas-phase fundamental experimental frequency of 1866.4 cm^{-1}.[2b] The B3LYP functional calculation gives a slightly longer Cu−H bond length (1.484 Å) and lower frequency (1879.1 cm^{-1}). The diatomic molecule CuH coordinates to H_2 and gives the coplanar (H_2)CuH complex, which is predicted to have the $^1A_1$ ground state. The Cu−H bond is elongated in this complex because of coordination by H_2 as calculated by both BPW91 and B3LYP functionals; however, the Cu−H stretching frequency is predicated to red-shift by 16 cm^{-1} (BPW91) or to blue shift by 5 cm^{-1} (B3LYP). In contrast, CuH_3 is a transition state with an imaginary bending frequency.

When two H_2 moieties associate with CuH, the higher order complex (H_2)$_2$CuH is obtained with C_s symmetry. However, this complex is predicted to be higher in energy than (H_2)CuH + H_2, and thus it cannot be formed in the low-temperature matrix. The (H_2)CuH_3 complex has two imaginary frequencies and lies 21.4 kcal/mol higher still. In contrast the (H_2)CuH species can combine another Cu atom to form (H_2)CuHCu, which is more stable than the sum of its parts. The H atom bridges two Cu atoms and one H_2 coordinates to one Cu atom, which gives a strong (H_2)-Cu stretching mode of 858.5 cm^{-1} at the BPW91 level: the B3LYP functional calculates similar results. Structures for copper hydrides are illustrated in Figure 7.

The dihydride CuH_2 is calculated to be a stable minimum but higher in energy than ground-state Cu atom and a H_2 molecule. At the BPW91/SDD level the bent $^2B_2$ structure with Cu−H bond length of 1.527 Å and H−Cu−H bond angle of 122.6° is 8 kcal/mol higher in energy than Cu + H_2. At the BPW91 level with the all-electron basis the CuH_2 bond length and angle are unchanged and the energy is 9 kcal/mol above Cu + H_2. Earlier SCF calculations find the same bent state described here.[20a] Optimization of the complex Cu(H_2) failed because of repulsive interaction between Cu and H_2. However Cu dimer can form a stable Cu$_2$(H_2) complex with end-on bonding to Cu_2 to H_2. The H−H bond is elongated by 0.045 Å the same as in (H_2)CuH, according to BPW91 calculation, indicating a strong interaction in this complex, which is more stable than $(CuH)_2$. A similar structure with a slightly longer Cu−Cu bond has been computed for $Cu_2H_2^+$.[21] Finally, we also compute CuHCu and CuCuH and their anions to help assign new spectral bands and these results are given in Table 4.

Similar calculations have been performed for silver hydrides and the results are listed in Table 5. The Ag−H bond lengths in AgH and (H_2)AgH are slightly longer than Cu−H bond lengths, and as a result the Ag−H stretching frequencies are red-shifted about 100 cm^{-1} from Cu−H. However when two H_2 are coordinated to AgH, the global minimum appears to be (H_2)AgH_3 with C_{2v} symmetry, which is different from the copper counterpart, but analogous to (H_2)AuH_3,[7] although (H_2)AgH_3 is coplanar. We note that (H_2)AgH_3 is 33 kcal/mol (BPW91) or 39 kcal/mol (B3LYP) higher energy than H_2 + (H_2)AgH. Structures for silver hydrides are shown in Figure 8. Since silver appears to cluster,[22] calculations were also done for AgAgH, Ag−H−Ag, and their anions.

Computations were done for gold hydrides in our earlier work,[7] and here we report new calculations for AuAuH, AuHAu and their anions (Table 6), which find the AuAuH forms to be more stable. DFT calculations for AuH_2 accurately predict the bending mode observed here: higher level calculations are suggested to confirm this experimental observation.

We also include a systematic investigation of the coinage metal MH and MD molecules comparing the SDD and LANL2DZ pseudopotentials and basis sets[11c,d] (Table 7).

Discussion

New group 11 hydrides will be identified from isotopic substitution and matrix host effects on their infrared spectra and from comparison to frequencies calculated by DFT.

CuH, AgH, and AuH. A band at 1879.8 cm^{-1} appeared on laser-ablated Cu atom deposition with H_2 in argon, which shifts to 1354.9 cm^{-1} with D_2 giving a 1.387 H/D isotopic ratio. With HD both bands were observed unshifted suggesting the diatomic CuH and CuD assignments. In solid neon the absorption for CuH was split into two sites at 1894.4 and 1889.9 cm^{-1}, and the stretching frequency of CuD was identified at 1362.2 cm^{-1}. These absorptions are slightly blue shifted from the gas-phase value[2] of 1866.4 cm^{-1} because of matrix repulsion as observed for AuH.[7]

A sharp absorption for AgH was observed at 1717.0 cm^{-1} on deposition in argon, which increased on photolysis and disappeared on annealing to 25 K. The counterpart absorption of AgD shifts to 1233.8 cm^{-1}, and gives the H/D isotopic frequency ratio 1.392. Moreover these same bands were observed in HD experiments (Figure 4) supporting the AgH and AgD assignments. No counterparts were observed in solid neon. The argon matrix value is blue shifted 25 cm^{-1} from the 1691.7 cm^{-1} gas-phase value.[5]

The results of DFT calculations for CuH and AgH are summarized in Tables 3 and 4 using the SDD pseudopotential and basis. The B3LYP functional frequency calculations are in excellent agreement with the gas phase values for CuH and AgH, and the BPW91 functional gives slightly higher frequencies: the same is found for AuH.[7] It is interesting to compare the bond lengths and stretching frequencies of coinage metal monohydrides here. The calculated bond length increases from Cu−H to Ag−H but decreases from Ag−H to Au−H, which is in line with the frequency observations at 1879.8 cm^{-1} (CuH), 1717.0 cm^{-1} (AgH), and 2226.6 cm^{-1} (AuH),[7] respectively, in solid argon. The relativistic bond-length contraction plays an important role for this chemical property trend.[23]

A previous investigation favored the BPW91 functional over B3LYP for frequencies, but the LANL2DZ pseudopotential and basis was employed for the metals.[8e] We found better frequency fits with the SDD pseudopentials for palladium and platinum hydrides and dihydrogen complexes,[24] and the same is also true for AuH but not AgH and CuH. Table 7 compares gas-phase anharmonic frequencies (observed $v = 0$ to $v = 1$ fundamentals)[2b] and calculated harmonic frequencies for the group 11 MH and MD molecules all using the 6-311++G(d,p) hydrogen basis. The percent deviations for MH and MD are, of course, different because the observed frequencies are anharmonic and the calculated values are harmonic, but the purpose of this exercise is to fit observed frequencies by calculation.

TABLE 4: Calculated Structures and Vibrational Frequencies (cm^{-1}) for Copper Hydrides and Dihydrogen Complexes

species	state	Å or deg	frequencies, cm^{-1} (symmetry, intensities, km/mol)
			BPW91/6-311++G(d,p)/SDD
CuH	$^1\Sigma^+$	CuH: 1.456	CuH: 1947 (26). CuD: 1388 (13)
CuH_2	$^2B_2$	CuH: 1.527 HCuH: 122.6	CuH_2: 1770 (a_1, 7), 1631 (b_2, 5), 637 (a_1, 75)
CuH_2^- [a]	$^1\Sigma_g^+$	CuH: 1.560	CuH_2^-: 1687 (σ_g, 0), 1501 (σ_u, 838), 643 (π_u, 177 × 2) $CuHD^-$: 1601 (330), 1122 (295), 560 (130 × 2) CuD_2^-: 1187 (0), 1078 (413), 462 (83 × 2)
$(H_2)CuH$	$^1A_1$	CuH: 1.481 CuH′: 1.723 H′H′: 0.794	$(H_2)CuH$: 3671 (a_1, 5), 1931 (a_1, 40), 1185 (b_2, 7), 768 (a_1, 1), 514 (b_1, 37), 445 (b_2, 58) $(D_2)CuD$: 2597 (3), 1375 (20), 841 (3), 552 (0), 371 (19), 320 (29)
CuH_3 (C_{2v})	$^1A_1$	CuH: 1.521 CuH′: 1.410 HCuH′: 82.2	2152 (a_1, 13), 1848 (a_1, 2), 1739 (b_2, 394), 793 (b_1, 36), 697 (a_1, 29), 677i (b_2, 555)
$(H_2)_2CuH$	$^1A_1$	CuH: 1.722 CuH′: 1.518 CH″: 1.790 H′H″: 0.806 HCuH′: 115.6 H′CuH″: 142.0	3488 (95), 3464 (159), 1876 (107), 1165 (25), 1126 (32), 774 (29), 702 (0), 546 (27), 537 (0), 372 (29), 273 (3), 260 (29)
$CuCu(H_2)$ [b] (C_{2v})	$^1A_1$	CuH: 1.748 HH: 0.794 CuCu: 2.256	3665 (a_1, 15), 1033 (b_2, 19), 726 (a_1, 8), 258 (a_1, 2), 208 (b_1, 10), 171 (b_2, 8)
$(CuH)_2$ [b]	$^1A_1$	CuH: 1.754 CuCu:2.168	1411 (a_1, 0), 1196 (a_1, 281), 602 (b_1, 95), 507 (b_2, 316), 359 (b_2, 0), 317 (a_1, 0)
$(H_2)CuHCu$	$^2A'$	CuH:1.723 CuCu′: 2.366 Cu′H: 1.545 Cu′H′: 1.660 Cu′H″: 1.674 H′H″: 0.822 HCu′H′: 164.4	$(H_2)CuHCu$: 3222 (a′, 1349), 1624 (a′, 2), 1325 (a′, 86), 903 (a′, 12), 858 (a′, 145), 476 (a″, 2), 378 (a″, 0), 188 (a′, 17), 187 (a′, 9) $(D_2)CuDCu$: 2279 (674), 1156 (2), 938 (43), 644 (7), 618 (70), 341 (1), 271 (0), 185 (9), 137 (8)
$(H_2)CuCu(H_2)$ (D_{2d})	$^1A_1$	CuCu: 2.273 CuH: 1.808 HH: 0.784	3798 (a_1, 0), 3792 (b_2, 18), 834 (e, 19 × 2), 604 (a_1, 0), 524 (b_2, 39), 256 (a_1, 0), 211 (e, 4 × 2), 157 (3, 13 × 2), 137 (b_1, 0)
CuHCu [c]	$^2\Sigma_u^+$	CuH: 1.550	1955 (σ_u, 531), 195 (σ_g, 0), 75i (π, 47 × 2)
$CuHCu^-$ [c]	$^1\Sigma_g^+$	CuH: 1.611	1610 (σ_u, 702), 421 (π_u, 27 × 2), 170 (σ_g, 0)
CuCuH	$^2A'$	CuH: 1.489 CuCu: 2.317 CuCuH: 131.7	1791 (64), 274 (90), 199 (4)
$CuCuH^-$ [c]	$^1\Sigma^+$	CuH: 1.530 CuCu: 2.373	1657 (612), 347 (35 × 2), 199 (4)
			B3LYP/6-311++G(d,p)/SDD
CuH	$^1\Sigma$	CuH:1.460	CuH: 1922 (50). CuD: 1371 (25)
CuH_2	$^2B_2$	CuH:1.525 HCuH: 121.5	CuH_2: 1792 (a_1, 9), 1645 (b_2, 17), 658 (a_1, 8)
CuH_2^-	$^1\Sigma_g^+$	CuH: 1.562	CuH_2^-: 1666 (σ_g, 0), 1492 (σ_u, 919), 654 (π_u, 242 × 2)
$(H_2)CuH$	$^1A_1$	CuH: 1.480 CuH′: 1.756 H′H′: 0.775	$(H_2)CuH$: 3933 (a_1, 0), 1928 (a_1, 61), 1117 (b_2, 6), 727 (a_1, 0), 493 (b_1, 54), 434 (b_2, 75) $(D_2)CuD$: 2782 (0), 1373 (31), 791 (3), 522 (0), 356 (27), 312 (38)
$CuCu(H_2)$ [b] (C_{2v})	$^1A_1$	CuH: 1.848 HH: 0.769 CuCu: 2.281	4026 (a_1, 5), 778 (b_2, 20), 468 (a_1, 34), 243 (a_1, 1), 176 (b_1, 9), 146 (b_2, 6)
$(CuH)_2$ [b]	$^1A_1$	CuH: 1.758 CuCu: 2.193	1408 (a_1, 0), 1182 (b_1, 344), 625 (a_1, 135), 501 (b_2, 476), 297 (a_1, 0), 294 (a_2, 0)
$(H_2)CuHCu$	$^2A'$	CuH: 1.755 CuCu′: 2.401 Cu′H: 1.534 Cu′H′: 1.689 Cu′H″: 1.700 H′H″: 0.796 HCu′H′: 164.4	$(H_2)CuHCu$: 3560 (a′, 1200), 1658 (a′, 2), 1270 (a′, 65), 837 (a′, 40), 831 (a′, 136), 481 (a″, 5), 351 (a″, 0), 187 (a′, 16), 166 (a′, 12) $(D_2)CuDCu$: 2518 (600), 1181 (1), 899 (32), 601 (47), 595 (39), 344 (2), 251 (0), 164 (13), 137 (8)
$(H_2)CuCu(H_2)$ (D_{2h})	^1A_g	CuCu: 2.289 CuH: 1.923 HH: 0.763	4115 (a_g, 0), 4111 (b_{1u}, 14), 675 (b_{3g}, 0), 670 (b_{2u}, 36), 450 (a_g, 0), 388 (b_{1u}, 101), 245 (a_g, 0), 174 (b_{2g}, 0), 149 (b_{3g}, 0), 147 (b_{3u}, 17), 124 (b_{2u}, 13), 72 (a_u, 0)
CuHCu [c]	$^2\Sigma_u^+$	CuH: 1.561	1857 (σ_u, 1023), 1909 (σ_g, 0), 186 (π_u, 66 × 2)
$CuHCu^-$ [c]	$^1\Sigma_g^+$	CuH: 1.618	1514 (σ_u, 1199), 456 (π_u, 35 × 2), 166 (σ_g, 0)
CuCuH [d]	$^2A'$	CuH: 1.486 CuCu: 2.343 CuCuH: 128.9	1791 (92), 282 (107), 96 (5)
$CuCuH^-$ [d]	$^2\Sigma^+$	CuH: 1.534 CuCu: 2.398	1640 (σ, 732), 349 (π, 56 × 2), 189 (σ, 5)

[a] The CuH_2^- anion is more stable than CuH_2 by 54 kcal/mol (BPW91) or 51 kcal/mol (B3LYP). [b] All-electron basis: $CuCu(H_2)$ is lower than $(CuH)_2$ by 12 kcal/mol with BPW91 and 11 kcal/mol with B3LYP. [c] The $CuHCu^-$ anion is lower energy than CuHCu by 33 kcal/mol (BPW91) or 31 kcal/mol (B3LYP), and the $CuCuH^-$ anion is 51 kcal/mol lower than CuCuH(BPW91). [d] The $CuCuH^-$ anion is 53 kcal/mol lower than CuCuH (B3LYP). CuHCu is 2 kcal/mol lower than CuCuH, and $CuCuH^-$ is 21 kcal/mol lower than $CuHCu^-$ (B3LYP).

TABLE 5: Calculated Structures and Vibrational Frequencies (cm^{-1}) for Silver Hydrides and Hydrogen Complexes

species	state	structure Å or deg	frequencies, cm^{-1} (symmetry, intensities, km/mol)
		BPW91/6-311++G(d,p)/SDD	
AgH	$^1\Sigma^+$	AgH: 1.608	AgH: 1803.8 (43). AgD: 1281.9 (22)
AgH_2	$^2B_2$	AgH: 1.655 HAgH: 120.3	1683.1 (a_1, 5), 1540.6 (b_2,1), 537.4 (a_1, 74)
AgH_2^- [a]	$^1\Sigma_g^+$	AgH: 1.699	1618.7 (σ_g, 0), 1444.7 (σ_u, 931), 619.5 (π_u, 167 × 2)
$(H_2)AgH$	$^1A_1$	AgH: 1.617 AgH′: 1.973 H′H′: 0.779	$(H_2)AgH$: 3905.6 (a_1, 5), 1859.5 (a_1, 53), 920.1 (b_2, 5), 590.5 (a_1, 2), 440.2 (b_1, 47), 393.4 (b_2, 62) (HD)AgH: 3384.3 (5), 1859.4 (54), ... (HD)AgD: 3384.2 (5), 1321.4 (27), ... $(D_2)AgD$: 2762.8 (3), 1321.1 (27), 651.8 (2), 421.6 (1), 314.9 (24), 280.9 (31)
AgH_3	$^1A_1$	AgH: 1.652 AgH′: 1.535 H′AgH: 84.8	2080.7 (a_1, 4), 1861.4 (a_1, 1), 1726.0 (b_1, 517), 783.1 (b_2, 28), 752.8 (a_1, 21), 413.0i (b_1, 383)
$(H_2)AgH_3$	$^1A_1$	AgH: 1.647 AgH′: 1.551 AgH″: 1.888 HAgH′: 83.5 HAgH″: 84.2, 108.8	3513.9 (a_1, 11), 2091.7 (a_1, 1), 1874.6 (a_1, 1), 1745.1 (b_1, 429), 1255.8 (b_1, 12), 788.6 (a_1, 0), 766.0 (b_2, 20), 688.3 (a_1, 0), 577.5 (a_2, 0), 518.3 (b_2, 4), 427.3 (b_1, 231), 398.1 (b_1, 1)
AgAgH	$^2A'$	AgH: 1.631 AgAg: 2.683	1708 (90), 251 (110), 137 (1)
$AgAgH^-$	$^1\Sigma^+$	AgH: 1.673 AgAg: 2.698	1587 (691), 318 (51 × 2), 141 (3)
$AgHAg^-$	$^1\Sigma_g^+$	AgH: 1.779	1435 (σ_u, 711), 422 (π_u, 43 × 2), 122 (σ_g, 0)
		B3LYP/6-311++G(d,p)/SDD	
AgH	$^1\Sigma$	AgH: 1.620	AgH: 1775.2 (65) AgD: 1261.6 (33)
AgH_2	$^2B_2$	AgH: 1.662; HAgH: 119.1	1642.6 (a_1, 4), 1507.6 (b_2, 4), 521.9 (a_1, 84)
AgH_2^- [a]	$^1\Sigma_g^+$	AgH: 1.706	1593.8 (σ_g, 0), 1428.5 (σ_u, 987), 617.4 (π_u, 217 × 2)
$(H_2)AgH$	$^1A_1$	AgH: 1.623 AgH′: 2.019 H′H′: 0.765	$(H_2)AgH$: 4093.7 (a_1, 16), 1836.1 (a_1, 77), 869.0 (b_2, 4), 570.4 (a_1, 4), 413.6 (b_1, 65), 377.4 (b_2, 78) $(D_2)AgD$: 2896.9 (8), 1304.6 (39), 615.4 (2), 407.4 (2), 295.8 (33), 269.6 (39)
$(H_2)AgH_3$	$^1A_1$	AgH: 1.645 AgH′: 1.540 AgH″: 1.933 HAgH′: 83.2 HAgH″:85.1, 108.6	3786.4 (a_1, 1), 2129.7 (a_1, 1), 1892.9 (a_1, 0), 751.2 (b_1, 506), 1175.4 (b_1, 12), 777.4 (b_2, 26), 725.3 (a_1, 1), 682.1 (a_1,2), 530.5 (a_2, 0), 497.5 (b_2, 6), 405.6 (b_1, 41), 392.5 (b_1, 252)
$AgHAg$ [b]	$^2\Sigma_u^+$	AgH: 1.738	1545 (σ_u, 1045), 219 (π_u, 76 × 2), 131 (σ_g, 0)
$AgHAg^-$ [b]	$^1\Sigma_g^+$	AgH: 1.794	1374 (σ_u, 1161), 417 (π_u, 47 × 2), 120 (σ_g, 0)
AgAgH [c]	$^2A'$	AgH: 1.642 AgAg: 2.723 AgAgH: 131.3	1667 (a′, 95), 222 (a′, 137), 127 (a′, 3)
$AgAgH^-$ [c]	$^1\Sigma$	AgH: 1.684 AgAg: 2.727	1555 (σ, 783), 316 (π, 67 × 2), 137 (σ, 3)

[a] The AgH_2^- anion is more stable than AgH_2 by 62 kcal/mol (BPW91) or 66 kcal/mol (B3LYP). [b] The $AgHAg^-$ anion is lower energy than AgHAg by 34 kcal/mol (B3LYP). AgHAg is more stable than AgAgH by 4 kcal/mol (B3LYP). [c] The $AgAgH^-$ anion is 56 kcal/mol (BPW91) or 58 kcal/mol (B3LYP) lower energy than AgAgH (B3LYP). AgHAg is 4 kcal/mol lower than AgAgH, but $AgAgH^-$ is 17 kcal/mol lower than $AgHAg^-$ (B3LYP).

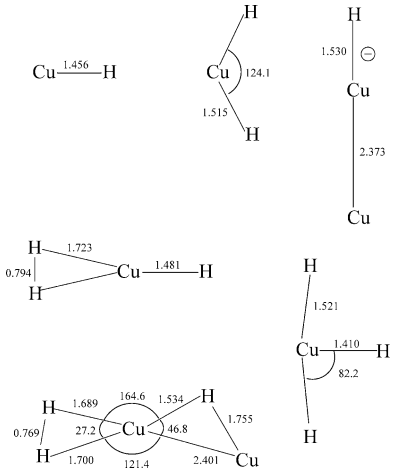

Figure 8. Structures calculated for copper hydrides at the BPW91/6-311++G(d,p)/SDD level.

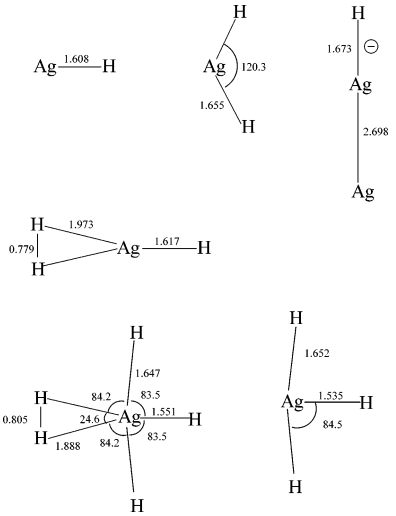

Figure 9. Structures calculated for silver hydrides at the BPW91/6-311++G(d,p)/SDD level.

In the case of AuH and AuD all but one of the calculated frequencies are high from 0.0 to 1.9% and the B3LYP/SDD value for AuD is low by 0.8%. The LANL2DZ frequencies are 0.5 to 0.8% higher than the SDD frequencies, which amounts to 10−15 cm^{-1} closer fit for the SDD calculation. The fit is clearly not as good for AgH and AgD, but LANL2DZ works a few % better than SDD. Deviations for CuH and CuD

TABLE 6: Calculated Structures and Vibrational Frequencies (cm^{-1}) for Gold Hydride Anions

species	state	structure, Å or deg	frequencies, cm^{-1} (symmetry, intensities, km/mol)
		BPW91/6-311++G(d,p)/SDD	
AuAuH[a]	$^2A'$	AuH: 1.571 AuAu: 2.645 AuAuH: 138.1	2086 (54), 277 (58), 135 (0)
$AuAuH^-$[a]	$^1\Sigma^+$	AuH: 1.602 AuAu: 2.686	1987 (σ, 527), 394 (π, 4 × 2), 133 (σ, 3)
AuHAu[b]	$^2\Sigma_u^+$	AuH: 1.672	1181 (σ_u, 483), 1245 (σ_g, 0), 243i (π_u, 20 × 2)
$AuHAu^-$[b]	$^1\Sigma_g^+$	AuH: 1.727	1542 (σ_u, 1703), 443 (π_u, 28 × 2), 110 (σ_g, 0)
		B3LYP/6-311++G(d,p)/SDD	
AuAuH[a]	$^2A'$	AuH: 1.570 AuAu: 2.680 AuAuH: 136.2	2092 (76), 302 (77), 125 (0)
$AuAuH^-$[a]	$^1\Sigma^+$	AuH: 1.605 AuAu: 2.710	1973 (σ_u, 567), 396 (π_u, 8 × 2), 128 (σ_g, 0)
AuHAu[b]	$^2\Sigma_u^+$	AuH: 1.678	1766 (σ_u, 676), 123 (σ_g, 0), 191i (π_u, 30 × 2)
$AuHAu^-$[b]	$^1\Sigma_g^+$	AuH: 1.732	1473 (σ_u, 2192), 460 (π_u, 33 × 2), 109 (σ_g, 0)

[a] $AuAuH^-$ is lower energy than AuAuH by 74 kcal/mol (BPW91) or 76 kcal/mol (B3LYP). [b] AuHAu is a transition state, but $AuHAu^-$ is lower in energy by 62 kcal/mol (BPW91) or 59 kcal/mol (B3LYP). The $AuAuH^-$ anion is more stable than the $AuHAu^-$ anion by 13 kcal/mol (BPW91) or by 16 kcal/mol (B3LYP).

TABLE 7: Comparison of Observed and Calculated Vibrational Frequencies (cm^{-1}) for Coinage Metal MH and MD Molecules

	AuH	AuD	AgH	AgD	CuH	CuD
observed[a]	2218.7	1591.7	1691.7	1216.5	1866.4	1346.1
BPW91/LAN[b]	2260.0	1602.7	1735.7	1233.5	1883.3	1342.7
Δ[c]	(+1.9%)[c]	(+0.7%)	(+2.6%)	(+1.4%)	(+0.9%)	(−0.3%)
B3LYP/LAN[b]	2244.7	1591.9	1706.0	1261.6	1848.0	1317.5
Δ[c]	(+1.2%)	(+0.0%)	(+0.8%)	(+3.7%)	(−1.0%)	(−2.2%)
BPW91/SDD	2250.5	1596.0	1803.8	1281.9	1947.1	1388.1
Δ[c]	(+1.4%)	(+0.3%)	(+6.6%)	(+5.4%)	(4.3%)	(+3.1%)
B3LYP/SDD	2227.4	1579.6	1775.2	1261.6	1922.5	1370.6
Δ[c]	(+0.4%)	(−0.8%)	(+4.9%)	(+3.7%)	(+3.0%)	(+1.8%)
BPW91/all[d]					1909.1	1361.0
Δ[c]					(+2.3%)	(+1.1%)
BPW91/all/plus[e]					1884.6	1343.6
Δ[c]					(+1.0%)	(−0.2%)
B3LYP/all[d]					1879.1	1339.7
Δ[c]					(+0.7%)	(−0.5%)
B3LYP/plus[f]					1913.8	1364.4
Δ[c]					(+2.5%)	(+1.3%)

[a] Gas-phase fundamental frequencies, $\omega_e - 2\omega_e x_e + 3.25\omega_e y_e$: data from ref 2b. [b] LANL2DZ pseudopotential and basis for metal and 6-311++G(d,p) for hydrogen. [c] Calculated minus observed expressed as percent of observed frequency. [d] All electron 6-311++G(d,p) basis for copper and hydrogen. [e] Larger all electron 6-311++G(3df, 3pd) for Cu and for H. [f] Larger 6-311++G(3df, 3pd) basis for H and SDD for Cu.

frequencies ranged from −2.2 to +4.3% and LANL2DZ is slightly better than SDD. The all-electron 6-311++G(d,p) basis for CuH and CuD gave even better results for frequencies than either pseudopotential: the BPW91 deviations were 2.3% for CuH and 1.1% for CuD, and the B3LYP differences are 0.7% for CuH and −0.5% for CuD. The larger H basis 6-311++G-(3df, 3pd) and SDD pseudopotential combination did almost as well with B3LYP: the computed frequencies were 2.5% high for CuH and 1.3% high for CuD.

(H_2)CuH, (H_2)AgH, and (H_2)AuH. All of the hydrogen [deuterium] matrix experiments produced the MH [MD] molecules in high yield, but these were necessarily trapped as (H_2)-MH [(D_2)MD] complexes. The 1862.5 cm^{-1} band in the argon matrix (Figure 1) appeared in the Cu−H stretching region on deposition, doubled its intensity on annealing to 15 K, but decreased on broadband photolysis in favor of CuH, and then restored on further annealing with the demise of CuH. The D counterpart for this band was observed at 1343.2 cm^{-1}. In HD experiments two bands at 1862.7 and 1343.0 cm^{-1} show very small isotopic shifts, indicating Cu−H and Cu−D stretching vibrations are slightly perturbed by another HD molecule. Experiments with $H_2 + D_2$ gave two broad bands centered at 1862.5 and 1343.2 cm^{-1}. These absorptions show similar isotopic substitution behavior as CuH and assignment to the (H_2)CuH complex immediately comes into mind. This identification is substantiated by observation of weak 3566.6 and 2582.0 cm^{-1} absorptions for the H−H and D−D stretching modes in the (H_2)CuH and (D_2)CuD complexes, respectively, in pure H_2 and D_2, which are associated with the stronger Cu−H and Cu−D stretching modes at 1861.4 and 1341.6 cm^{-1} (Figure 3). An associated 441 cm^{-1} band is assigned to the (H_2)Cu−H bending mode.

A similar assignment for (H_2)AgH can be made in solid argon, neon, hydrogen and deuterium. In solid argon, the 1735.8 and 1746.5 cm^{-1} bands appeared on deposition and increased on annealing to 20 K, decreased on broadband photolysis with increase in AgH, but further annealing recovered their intensities with loss of AgH. The deuterium counterparts were observed at 1247.2 and 1257.6 cm^{-1} with the same annealing and photolysis behavior. With HD two analogous bands at 1735.8 and 1748.2 cm^{-1} in the AgH stretching region and two analogous bands at 1247.4 and 1256.9 cm^{-1} in Ag−D stretching region were identified. The sharp 1746.5 and 1257.6 cm^{-1} features exhibited +1.7 and −0.7 cm^{-1} shifts with HD in solid

argon. In pure hydrogen and deuterium strong Ag−H(D) bands are observed at 1742.6 and 1255.7 cm^{-1} (Figure 5), with weaker associated H−H(D−D) stretching bands at 3805.9 and 2736.3 cm^{-1}. With pure $H_2 + D_2$, strong bands were observed at 1746.4, 1744.3 cm^{-1} and at 1255.9, 1253.7 cm^{-1} for the four isotopic complexes. These strong bands shift to 1748.6 and 1255.4 cm^{-1} for (HD)AgH and (HD)AgD, and a weak H−D stretching mode is observed unsplit at 3367.1 cm^{-1} in pure HD.

The Au−H stretching mode for the (H_2)AuH complex was observed at 2173.6 cm^{-1} with site at 2170.6 cm^{-1} in argon and at 2170.1 cm^{-1} in neon.[7] This assignment is further substantiated by pure H_2, D_2, HD, and $H_2 + D_2$ experiments. The absorptions at 2164.0 cm^{-1} in pure H_2 (Figure 6) and at 1556.5 cm^{-1} in pure D_2 are slightly lower than argon and neon values probably due to the van der Waals interaction between environmental H_2 and the (H_2)AuH molecule. The $H_2 + D_2$ experiments gave a doublet at 2163.7 and 2156.6 cm^{-1} in the upper Au−H stretching region, which corresponds to (H_2)AuH and (D_2)AuH, and at 1561.0 and 1556.3 cm^{-1} in the lower Au−D stretching region, which are due to (H_2)AuD and (D_2)AuD, respectively. The relative intensities of these upper and lower doublets was 5/1, which demonstrates a faster reaction of Au with H_2 than with D_2 under the same conditions. This is found in both laser-ablation and thermal gold-photolysis experiments. Furthermore, the coupling between (H_2)AuH and (D_2)AuH resulting in a 7.1 cm^{-1} splitting (and the like coupling between (H_2)AuD and (D_2)AuD resulting in a 4.7 cm^{-1} separation) are well predicted by our BPW91 calculations as 6.5 (5.4) cm^{-1}. With pure HD two strong bands at 2162.7 and 1555.2 cm^{-1} (Figure 6) and two weak bands at 3026.0 and 3022.3 cm^{-1} were observed, which exhibit similar intensity behavior and can be assigned to (HD)AuH and (HD)AuD. In the case of (H_2)AuH and (D_2)AuD the calculated H−H and D−D stretching mode intensities are zero, and no such bands are observed, but the H−D mode intensity is calculated as $^1/_8$ and $^1/_4$ of the Au−H and Au−D modes, respectively, and the observed bands fit nicely for the H−D stretching modes of (HD)AuH and (HD)AuD.

Two additional modes for the (H_2)AuH complex are observed, namely the in-plane (H_2)Au−H bending mode at 576.0 cm^{-1} (counterpart to 434.8 cm^{-1} for (D_2)AuD) and the antisymmetric H_2−AuH stretching mode at 1314.4 cm^{-1} (counterpart to 939.6 cm^{-1} for (D_2)AuD). The mixed $H_2 + D_2$ experiment reveals a 1314.6, 1294.3, 948.9, 939.6 cm^{-1} quartet for the upper band and weak 575.8, strong 560.2, weak 434.4 cm^{-1} absorptions for the lower band. Our DFT calculations show that intensity increases for the D_2Au−H bending mode, but decreases for the H_2Au−D bending mode: hence, the former is intensified, and the latter is not observed.

On the basis of the lower calculated symmetric (H_2)−AuH stretching mode and lower observed antisymmetric H_2−AuH stretching mode, as compared to the analogous higher (H_2)Pd vibrations,[24] (H_2) is more weakly bound to AuH than to Pd. The 1431.5 cm^{-1} band observed in both laser ablation and thermal gold experiments is probably due to a combination band for (H_2)AuH.

DFT frequency calculations support these assignments. With the BPW91 functional the M−H modes for the (H_2)MH complexes (M = Cu, Ag, Au) are predicted at 1931.3, 1859.5, and 2205.9 cm^{-1}, which are overestimated by 3.8%, 6.7%, and 1.6%, respectively. The BPW91 functional predicts a 16 cm^{-1} red shift for (H_2)CuH from CuH and a 17 cm^{-1} red shift is observed whereas this calculation predicts a 56 cm^{-1} blue shift for Ag−H in (H_2)AgH and a 30 cm^{-1} blue shift is observed. In the gold case, a 58 cm^{-1} red shift is predicted and a 55 cm^{-1} red shift is observed.[7] It is gratifying that the DFT calculations correctly predicted the blue shift observed for the Ag−H mode in (H_2)AgH. From the calculated H−H bond lengths in the (H_2)MH complexes, 0.794, 0.779, and 0.807 Å for Cu, Ag, and Au, respectively, one can see that the interaction with (H_2) varies AuH > CuH > AgH.

Confirmation of the (H_2)MH complex identification is found in the observation of weak H−H stretching modes for the Cu and Ag hydride complexes and the agreement with frequencies predicted by DFT. The BPW91 functional predicts H−H and D−D stretching modes at 3670.9 and 2597.0 cm^{-1} for (H_2)CuH and (D_2)CuD with 13−15% of the Cu−H and Cu−D mode intensities. The observed bands at 3566.6 and 2582.0 cm^{-1} are in excellent agreement although the relative intensities are an order-of-magnitude weaker than calculated. Note that the observed 3566.6/2582.0 = 1.381 frequency ratio reveals anharmonicity, but the calculated 3670.9/2597.0 = 1.414 frequency ratio is harmonic. Similar agreement is found for the H−H(D−D) stretching modes of the Ag species observed at 3805.9 and 2736.3 cm^{-1} with 1.391 ratio. The CuH interaction with H_2 is clearly stronger than the AgH interaction as the H−H stretching mode is shifted 239 cm^{-1} lower and is more anharmonic and the computed H−H length is 0.015 Å longer. Unfortunately, the computed intensity for this mode in the (H_2)AuH complex is very low, and this mode is not observed but the H−D mode is observed in (HD)AuH and (HD)AuD.

$(H_2)AuH_3$. DFT calculations predict a stable coplanar $(H_2)AgH_3$ complex while AgH_3 is a transition state with an imaginary H−Ag−H bending mode. A very strong b_1 H−Ag−H stretching mode is computed at 1745.1 cm^{-1} and real bending mode at 427.3 cm^{-1} at the BPW91/6-311++G(d,p) level. The strongest band for AgH_3 is calculated at 1726.0 cm^{-1}. However one imaginary bending frequency is found for AgH_3, which can either rearrange to the more stable (H_2)AgH complex or be stabilized by coordinating another H_2 molecule to form $(H_2)AgH_3$. However, $(H_2)AgH_3$ is higher energy than $H_2 + (H_2)$AgH by 33 kcal/mol (BPW91) or 39 kcal/mol (B3LYP), and $(H_2)AgH_3$ is probably not formed in these experiments. On the other hand, the $(H_2)AuH_3$ complex is higher energy than $H_2 + (H_2)$AuH by much smaller amounts (19 kcal/mol, BPW91 and 23 kcal/mol, B3LYP), and the $(H_2)AuH_3$ complex is probably formed from excited AuH_3.[7]

In the Au + H_2 reactions a strong band at 1661.5 cm^{-1} band was observed as a major product in pure H_2, and the deuterium counterpart at 1198.6 cm^{-1} was identified in previous pure D_2 experiments.[7] With pure HD the two strong bands exhibit large blue-shifts to 1821.4 and 1267.1 cm^{-1}, as shown at the top of Figure 6, which are due to the almost identical long Au−H and Au−D bond stretching modes in the H−Au−D linkage for (HD)AuHDH and (HD)AuHDD. These bands are calculated to appear 6.5 and 4.5% above the antisymmetric pure isotopic bands owing to the higher unobserved pure isotopic symmetric stretching mode, and the observed bands are 9.6 and 5.7% higher. Very weak 1660.5 and 1195.4 cm^{-1} bands are just below the strong pure isotopic absorptions, and they are due to (HD)AuH_3 and (HD)AuD_3, respectively. The mixed isotopic spectrum observed in pure HD confirms the matrix identification of the higher $(H_2)AuH_3$ complex with a T-shaped AuH_3 subunit. In the $H_2 + D_2$ experiments strong bands were observed at 1663.7 and 1198.6 cm^{-1} for the "top" H−Au−H and D−Au−D modes in the (L)AuHHX and (L)AuDDX complexes. Both mixed precursor results show that the initial isotopic reagent (XY) molecules react with the AuH or AuD primary product to form XYAuH* and XYAuD*, which relax to (XY)AuH and (XY)-

AuD or form higher (XY)AuXYH and (XY)AuXYD complexes. The "XY" molecule makes the "top" of the T in the $(H_2)AuH_3$ complex.

Note that 265 nm irradiation in thermal gold experiments produces the 1666.8 (1205.9 cm^{-1}) satellite features and not the major 1661.5 (1198.6) absorptions for $(H_2)AuH_3$ ($(D_2)AuD_3$) observed in laser ablation experiments.[7]

AuH_2 and CuH_2. Ozin and co-workers have discussed the ^2P excitation and annealing for the $Cu/H_2/Kr$ matrix for the system where the photochemical reaction gave CuH and the annealing back reaction formed the Cu + H_2 reagents.[3b,c] We expect that pure hydrogen will be a better medium for the formation of these MH_2 molecules.

Our DFT calculations predict a strong H−Au−H bending mode in the 660 cm^{-1} region and very weak Au−H stretching modes for AuH_2.[7] The 638.1 cm^{-1} band observed in pure hydrogen for both laser-ablation[15] and thermal-photolysis gold experiments is assigned to the bending mode of AuH_2. The AuD_2 counterpart at 457.0 cm^{-1} (Figure 7B) defines a 1.396 H/D ratio, which is lower than the harmonic ratio 1.408 from DFT frequencies. Our HD experiment[15] produces an intermediate 570.6 cm^{-1} absorption for AuHD, which is also in agreement with DFT isotopic frequency calculations. The 570.6 cm^{-1} band is 23.1 cm^{-1} above the observed AuH_2/AuD_2 median, and the B3LYP frequency 579.1 cm^{-1} is 7.9 cm^{-1} above the calculated 666.5/473.4 median.[15] Balusubramanian and Laio calculate a barrier of 20 kcal/mol at the CASSCF level for the dissociation of AuH_2 to the lower energy Au + H_2 products.[20b]

With laser-ablated copper and pure hydrogen a weak band at 636.5 cm^{-1} increases slightly on $\lambda > 290$ nm photolysis (to $A = 0.002$), changes little on 240 nm irradiation and decreases on 6.5 K annealing. The pure deuterium counterpart at 458.5 cm^{-1} doubles on $\lambda > 240$ nm photolysis (to $A = 0.003$) (290 nm irradiation was not performed). These bands define a 1.388 H/D ratio. Copper in pure HD gave a weak 573.1 cm^{-1} absorption, which is appropriate for a bending vibration of a MH_2 unit. Our DFT calculations predict the bending mode of CuH_2 slightly lower than the bending mode of AuH_2 and a 1.398 harmonic H/D ratio as H and D move less against Cu than Au. The weak 636.5 (458.5) cm^{-1} bands are assigned to the bending modes of $CuH_2(CuD_2)$. Our observation of $CuHD^-$ in two pure HD experiments without CuH_2^- and CuD_2^- requires the formation of CuHD,[15] which is identified here by the weak 573.1 cm^{-1} band. The hydrogen (deuterium) matrix environment has made it possible to trap a small amount of CuH_2, whereas this was not possible in earlier solid krypton experiments.[3b] Although CuH_2 is higher energy than Cu + H_2, there is a barrier of approximately 20 kcal/mol to this dissociation calculated at the SCF level.[20a]

The group 11 hydrides observed in argon, neon, and hydrogen matrices, which allow progressively more diffusion and reaction of H_2, are summarized in Chart 1 (ann = annealing and major product underlined). The AgH_2 molecule is less stable than AuH_2, and it has a smaller 13 kcal/mol barrier to dissociation,[20c] and accordingly AgH_2 is not observed here.

$(H_2)CuHCu$. The 841.2 cm^{-1} band in the argon matrix tracking with a weak band at 1270.8 cm^{-1} displays unique properties: it appears on annealing to 25 K, disappears on full-arc photolysis, and recovers on further annealing to 30 K. These bands shift to 622.9 and 912.8 cm^{-1}, respectively, with D_2 in argon. Note that the 841.2 cm^{-1} band shows a low 1.351 H/D isotopic ratio but the 1270.8 cm^{-1} band exhibits a high 1.392 H/D ratio, suggesting different mode assignments for this molecule. The mixed isotopic substitution bands with H_2 + D_2 and HD are complicated: absorptions at 890.6 and 862.5 cm^{-1} in the upper region and 645.2 and 622.9 cm^{-1} in the lower region are observed for HD and the same band distributions are displayed for H_2 + D_2 in argon. Note that the 841.2 cm^{-1} band (all H band) does not appear, but the 622.9 cm^{-1} band (D band) does appear with other isotopic substitution bands in mixed isotopic experiments. The absorptions for this molecule in neon were observed at 847.3 cm^{-1} (H) and 628.2 cm^{-1} (D).

CHART 1

Argon	Neon	Hydrogen
CuH	CuH	CuH_2
ann $(H_2)CuH$	$\underline{(H_2)CuH}$	$(H_2)CuH$
AgH, AgAgH	AgAgH	AgAgH
$\underline{(H_2)AgH}$	$(H_2)AgH$	$(H_2)AgH$
AuH, AuAuH	AuAuH	$AuAuH$, AuH_2
ann $(H_2)AuH$	$\underline{(H_2)AuH}$, $(H_2)AuH_3$	$(H_2)AuH$, $\underline{(H_2)AuH_3}$

Similar absorptions were observed in pure hydrogen experiments: bands at 845.3 and 1284.3 cm^{-1} band observed after deposition increased on annealing to 5 K, but decreased on photolysis and reproduced on annealing to 6 K. Experiments with pure D_2 gave counterpart absorptions at 626.2 and 913.7 cm^{-1}. Three experiments were done with lower, medium, and higher laser-ablation energy, and the 626.2 cm^{-1} band was favored with higher energy. With pure HD and pure H_2 + D_2 four substituted bands due to this molecule were observed at 885.6, 844.8, 655.4, and 627.3 cm^{-1}, which shows the same behavior as found in the argon matrix.

The 1270.8 cm^{-1} band in argon and 1284.3 cm^{-1} band in pure H_2 show Cu−H stretching mode isotopic frequency ratios although this mode is located 600 cm^{-1} lower than the Cu−H diatomic stretching frequency. It can be inferred that this is a Cu−H stretching vibration perturbed by another Cu atom. Enhancement with higher laser-ablation energy suggests that two Cu atoms are involved in this molecule. The 841.2 cm^{-1} band with lower 1.3515 H/D ratio lies in the metal−H_2 or bridged metal−H−metal stretching region. However the HD spectra do not fit band distributions observed for other metal hydrides and hydrogen complexes. Here the theoretical calculations are extremely helpful to identify this molecule. The potential energy with two Cu and three, four, five, or six hydrogen atoms was explored extensively by BPW91 and B3LYP functionals, and the $(H_2)CuHCu$ molecule with C_s symmetry is the lowest in energy. A strong Cu−H_2 stretching mode predicted at 858.5 cm^{-1} (BPW91) and 830.8 cm^{-1} (B3LYP) is very close to experimental values of 841.2 cm^{-1} (argon) and 847.3 cm^{-1} (pure H_2). Moreover the calculated Cu−H stretching mode perturbed by another Cu atom at 1325.1 cm^{-1} (BPW91) and 1270.0 cm^{-1} (B3LYP) also fits experiment very well. The most important results from calculations are for HD substituted spectra; there are three isotopomers for Cu_2−H_2D and three for Cu_2−HD_2, but the two with (HD)CuHCu and $(D_2)CuHCu$ patterns are the lowest in energy, respectively. At the B3LYP level two stronger bands calculated at 681.4 and 833.6 cm^{-1} for (HD)CuHCu are slightly higher than 600.9 cm^{-1} for $(D_2)CuDCu$ and 830.8 cm^{-1} for $(H_2)CuHCu$. Of the two bands at 600.6 and 902.2 cm^{-1} for $(D_2)CuHCu$, one is essentially the same as for $(D_2)CuDCu$ and the another is a little higher. These calculated frequencies explain the experimental results exceptionally well.

Similar absorptions were observed in thermal Cu atom reactions with H_2 in solid argon, and the authors suggested an assignment to $(H_2)Cu(\mu\text{-}H)_2Cu(H_2)$.[25] However, our calculations find that the ring structure is less stable than $CuCu(H_2)$, and accordingly the former structure is very high energy. Furthermore, this identification is not compatible with HD isotopic substitution.

Metal Cluster Hydrides and Anions. Several absorptions in these experiments increase on annealing and are photosensitive, which invites consideration as metal cluster hydrides. In our earlier work bands at 2083 (1498) cm^{-1} for $H_2(D_2)$ in neon and 2076 (1485) cm^{-1} in argon were identified as $Au_xH(Au_xD)$.[7] We now add 2082 (1493) cm^{-1} for pure $H_2(D_2)$. Our DFT calculations find the stable AuAuH complex to have a strong absorption near 2090 cm^{-1}, which verifies this assignment for the above bands. Likewise the $AuAuH^-$ anion is predicted to absorb even more strongly near 1980 cm^{-1} and sharp 1991.7 (1434.5) cm^{-1} bands (ratio 1.388) in pure $H_2(D_2)$ increase on annealing and are appropriate for the $AuAuH^-$ anion. The HD reaction gives the same bands, which shows that a single H(D) is involved. Electrons formed in the laser ablation process are captured byproduct molecules in these experiments. Atomic gold has a large 53 kcal/mol electron affinity,[26] and Au^- could be a reagent in these experiments. Although the $AuHAu^-$ anion isomer is predicted to absorb very strongly near 1500 cm^{-1}, this isomer is 16 kcal/mol higher in energy and is not observed in these experiments.

A similar compound, $NaAu_2H_{1-x}$, has recently been prepared in the solid state as an intermediate in the reaction of 2Au and NaH.[27] This compound has the analysis $NaAu_2H_{0.66}$ at 260 °C and $NaAu_2H_{0.47}$ at 278 °C and releases all hydrogen above 300 °C. One might conjecture that $NaAu_2H$ containing the same Au_2H^- anion described above is formed first since the reaction begins at 200 °C, H_2 is released as the temperature is increased from 250 °C, and only $NaAu_2$ remains above 300 °C. The proposal of a metal hydride intermediate below 300 °C is also in agreement with contraction of the unit cell above 300 °C by X-ray analysis.[27]

Silver is known to cluster on deposition in matrix samples,[22] and new bands below AgH at 1691.9 (1216.3) cm^{-1} for $H_2(D_2)$ in argon, 1699 (1222) cm^{-1} bands in neon, and 1692 (1218) cm^{-1} bands in pure $H_2(D_2)$ are in very good agreement with our 1708 (1214) cm^{-1} BPW91 prediction for AgAgH.

With pure H_2 and Ag a weak band appeared at 1523 cm^{-1} on deposition, increased slightly on annealing and 380−700 nm photolysis, but disappeared on 290−700 nm irradiation with marked growth in the above 1692 cm^{-1} absorption. With pure D_2 this band shifts to 1101 cm^{-1} defining a 1.384 H/D ratio and with HD a weak 1523 cm^{-1} band was observed. This vibration was also observed in solid neon at 1516 (1097) cm^{-1}.

Our B3LYP calculation predicts very strong 1555 (1105) cm^{-1} bands for $AgAgH^-$ ($AgAgD^-$), which identify the last set of absorptions. Photodetachment of $AgAgH^-$ leads to growth of AgAgH; hence, the photochemical relationship between the 1692 and 1523 cm^{-1} absorptions. A very sharp, very photosensitive band was observed in pure D_2 at 955.9 cm^{-1} with a weak 1320.9 cm^{-1} H_2 counterpart: $\lambda > 380$ nm photolysis destroyed the 955.9 cm^{-1} band in favor of the 1101 cm^{-1} absorption assigned above to $AgAgD^-$. Our B3LYP calculation also finds a symmetrical $AgHAg^-$($AgDAg^-$) isomer with very strong 1374 (974) cm^{-1} absorptions. Even though the $AgHAg^-$ isomer is computed to be 20 kcal/mol higher, it could be formed by reaction of Ag^- and AgH and be separated by an energy barrier from $AgAgH^-$. Photolysis at $\lambda > 380$ nm allows rearrangement to the more stable form.

In pure hydrogen, with Cu a weak 1821 cm^{-1} band behaves appropriately for Cu_2H. Our B3LYP calculations predict that CuHCu is slightly lower energy than CuCuH and absorbs about 60 cm^{-1} below CuH, while CuCuH absorbs another 60 cm^{-1} lower. The weak 1821 cm^{-1} absorption is probably due to Cu−H−Cu but we cannot rule out CuCuH. The $CuCuH^-$ anion is predicted to be 21 kcal/mol more stable than $CuHCu^-$ and to absorb strongly near 1640 cm^{-1}. The new photosensitive 1627.7 cm^{-1} band is assigned to the $CuCuH^-$ anion.

Reaction Mechanisms. The reaction of ground-state Cu atom with H_2 to form diatomic CuH is computed (BPW91/6-311++G**/SDD) to be 38 kcal/mol endothermic. However ultraviolet excitation,[3b] glow discharge,[3a] and laser-ablated Cu atoms[28] provide sufficient excess energy (namely the $Cu(^2P)$ state) to activate the H−H bond and produce CuH. The experimental energy change for reaction 1 in the gas phase is 40 kcal/mol.[5]

$$Cu(^2S) + H_2(^1\Sigma_g^+) \rightarrow CuH(^1\Sigma^+) + H(^2S) \quad [\Delta E = 38 \text{ kcal/mol (BPW91)}]^{29} \quad (1)$$

The insertion of ground-state Cu into H_2 is also endothermic, by 8 kcal/mol at the BPW91 level; hence, ground state (^2S) Cu will not perform reaction 2a, but a host of excited doublet $3d^{10}$-4p and quartet $3d^9$4s4p copper states[30] produced by laser ablation[28] should activate reaction 2a, based on previous work[3] and the excited Zn reaction model.[31] Even though CuH_2 ($^2B_2$) is higher in energy than Cu + H_2, a considerable energy barrier is calculated for its dissociation.[20a]

$$Cu(^2S) + H_2(^1\Sigma_g^+) \rightarrow CuH_2(^2B_2) \quad [\Delta E = 8 \text{ kcal/mol}] \quad (2a)$$

$$CuH_2(^2B_2) \rightarrow CuH(^1\Sigma_g^+) + H(^2S) \quad [\Delta E = 30 \text{ kcal/mol}] \quad (2b)$$

The CuH intermediate from reaction 1 has two fates in the following reactions: CuH can complex H_2 to form $(H_2)CuH$, which is exothermic by 7 kcal/mol or combine another Cu to give Cu_2H. Both Cu_2H and $(H_2)CuH$ are observed, but (H_2)-CuH is dominant in pure hydrogen even though reaction 4 is more exothermic.

$$CuH + H_2 \rightarrow (H_2)CuH \quad [\Delta E = -7 \text{ kcal/mol}] \quad (3)$$

$$CuH + Cu \rightarrow CuHCu \quad [\Delta E = -22 \text{ kcal/mol}] \quad (4a)$$

$$Cu + CuH \rightarrow CuCuH \quad [\Delta E = -21 \text{ kcal/mol}] \quad (4b)$$

The cluster hydride CuCuH has a significant electron affinity and the $CuCuH^-$ anion is observed in these experiments. Copper atom also has an appreciable electron affinity (28 kcal/mol)[26] and Cu^- anions are probably formed in these experiments from ablated electrons. Reaction 7 is also favorable to form $CuCuH^-$.

$$CuCuH + e^- \rightarrow CuCuH^- \quad [\Delta E = -51 \text{ kcal/mol}] \quad (5)$$

$$Cu + e \rightarrow Cu^- \quad [\Delta E = -28 \text{ kcal/mol}] \quad (6)$$

$$Cu^- + CuH \rightarrow CuCuH^- \quad [\Delta E = -43 \text{ kcal/mol}] \quad (7)$$

Likewise $(H_2)CuH$ can also react further with H_2 or with Cu. The higher order hydrogen complex, $(H_2)_2CuH$ is a stable structure, but reaction 8 is endothermic by 4 kcal/mol, which apparently prevents formation of $(H_2)_2CuH$ in the low-temperature matrix. This is the reason the $(H_2)CuH$ is observed in all

matrices as a major product. The hydride $(H_2)CuH_3$ is also calculated, but two imaginary frequencies are found and the total energy for this structure is 21 kcal/mol higher. The (H_2)-CuH complex reacts further with Cu to give $(H_2)CuHCu$, which is exothermic (reaction 9). This reaction proceeds spontaneously in 20 K argon, 4 K neon, and pure H_2.

$$(H_2)CuH + H_2 \rightarrow (H_2)_2CuH \quad [\Delta E = 4 \text{ kcal/mol}] \quad (8)$$

$$(H_2)CuH + Cu \rightarrow (H_2)CuHCu \quad [\Delta E = -15 \text{ kcal/mol}] \quad (9)$$

Similar reactions are observed for $Ag + H_2$, and diatomic AgH and $(H_2)AgH$ are formed. The experimental energy change for reaction 1 with silver is 51 kcal/mol.[5] The $(H_2)AgH$ complex is the major reaction product in pure hydrogen. The AgAgH cluster hydride and its anion are also formed in these experiments.

$$Ag + H_2 \rightarrow AgH + H \quad [\Delta E = 52 \text{ kcal/mol (BPW91)}] \quad (10)$$

$$AgH + H_2 \rightarrow (H_2)AgH \quad [\Delta E = -3 \text{ kcal/mol}] \quad (11)$$

$$Ag + AgH \rightarrow AgAgH \quad [\Delta E = -13 \text{ kcal/mol}] \quad (12)$$

$$AgAgH + e^- \rightarrow AgAgH^- \quad [\Delta E = -56 \text{ kcal/mol}] \quad (13)$$

The analogous reactions have been described for gold.[7] The present 265 nm dielectric notch filtered photolysis of gold atoms in solid $H_2(D_2)$ employs the precise excitation of the $^2P_{1/2} \leftarrow {}^2S_{1/2}$ gold absorption measured by Gruen and Bates at 263 nm in solid deuterium[22] as summarized in reaction 14. In solid H_2-(D_2) the subsequent $(H_2)AuH$ complex formation is spontaneous. We note that growth of $HO_2(DO_2)$ on photolysis from O_2 impurity,[32] which confirms the formation of H(D) atoms.

$$Au(^2S) + H_2 \xrightarrow{265 \text{ nm}} Au(^2P) + H_2 \rightarrow AuH + H \quad (14)$$

The observation of AuH_2 in both laser-ablation and thermal-photolysis experiments from reaction 15 and from recombination of AuH and H, shows that a barrier exists between AuH_2 and the more stable $Au + H_2$ decomposition products as the AuH_2 product is also trapped here. As mentioned earlier, this barrier has been calculated as 20 kcal/mol.[20b] For gold the formation of the higher $(H_2)AuH_3$ complex appears to follow from excitation[2] of AuH in the $(H_2)AuH$ complex as 290 nm irradiation increases $(H_2)AuH_3$ more than $(H_2)AuH$ (Figure 6 (b)).

$$Au(^2P) + H_2 \rightarrow AuH_2(^2B_2) \xrightarrow{20 \text{ kcal/mol barrier}} Au + H_2 \quad (15)$$

$$H_2 + (H_2)AuH \xrightarrow{265 \text{ nm}} (H_2)AuH_3 \quad (16)$$

The net growth of $(D_2)AuD_3$ on annealing was not addressed in our earlier work:[7] This increase of the 1198.6 cm^{-1} absorption is more than coalescence with the 1205.9 cm^{-1} matrix site absorption. The laser-ablation experiment produces a high yield of H atoms in solid hydrogen and atomic hydrogen reactions contribute.[32] The yield of AuH_2 increases on annealing in laser-ablation experiments[15] and so does the absorbance of $(H_2)AuH_3$ (Figure 6). Thus, exothermic reactions 17 and 18 contribute to the product growth on annealing.

$$AuH + H \rightarrow AuH_2 \quad [\Delta E = -28 \text{ kcal/mol}] \quad (17)$$

$$H_2 + AuH_2 + H \rightarrow (H_2)AuH_3 \quad [\Delta E = -59 \text{ kcal/mol}] \quad (18)$$

Finally, the gold cluster complexes AuAuH and $AuAuH^-$ are observed. These reactions are more exothermic than those of their silver counterparts.

$$Au + AuH \rightarrow AuAuH \quad [\Delta E = -19 \text{ kcal/mol}] \quad (19)$$

$$AuAuH + e^- \rightarrow AuAuH^- \quad [\Delta E = -74 \text{ kcal/mol}] \quad (20)$$

It is interesting to note a preference for reaction with H_2 over D_2 in 50/50 pure mixed samples. The ratios of complexed MH/MD absorptions are 3/1, 2.5/1, and 5/1 for Cu, Ag, and Au, respectively. We also observed weak AuH_2 and no AuD_2 with mixed pure H_2 and D_2. These ratios should be higher because the condensation efficiency of H_2 is less than for D_2 and the solid samples surely contain more D_2 than H_2. This preference for H_2 over D_2 is the same for gold with laser ablation and with resonance photolysis of thermally deposited gold atoms and it applies to both $(H_2)AuH$ and AuH_2 products.

Conclusions

Laser-ablated Cu, Ag, and Au atoms react with H_2, to give the diatomic MH molecules as primary products, which react further with H_2 to form the $(H_2)MH$ complexes. Diatomic CuH gives absorption at 1879.8 cm^{-1} in argon and 1889.9 cm^{-1} in neon. The complex $(H_2)CuH$ is the more stable product, which is observed at 1862.5 cm^{-1} in argon, 1869.1 cm^{-1} in neon, and 3566.6, 1861.4 cm^{-1} in pure hydrogen. A weak 636.5 cm^{-1} absorption is also observed for CuH_2 in pure hydrogen. The $(H_2)CuH$ complex reacts further with Cu atom instead of H_2 to form $(H_2)CuHCu$, which was observed at 841.2 cm^{-1} (Ar), 847.3 cm^{-1} (neon), and 845.3 cm^{-1} (pure H_2).

The $(H_2)CuHCu$ species is of interest as a small copper hydride cluster that binds dihydrogen. One copper atom will not bind H_2, but our DFT calculations find that Cu_2 does bind H_2 to form $Cu_2(H_2)$ and we present experimental evidence for a similar species, namely $(H_2)CuHCu$ where the CuHCu subunit forms a 3-membered ring (Figure 8). The barrier for dissociative cemisorption of H_2 on copper metal surfaces is in the 0.5−0.7 eV range.[33] Hence, the present $(H_2)CuHCu$ complex with Cu−(H_2) stretching frequency near 800 cm^{-1} provides a model for the low energy attachment of H_2 to the copper surface.

Likewise AgH absorbs at 1717.0 cm^{-1} in solid argon and reacts further with H_2 to give $(H_2)AgH$, particularly in solid hydrogen where $(H_2)AgH$ is favored.

Gold forms $(H_2)AuH$, $(H_2)AuH_3$, and AuH_2 in solid hydrogen, and these identifications are substantiated by D_2, $H_2 + D_2$, and HD substitution.[15] Complementary experiments with thermally evaporated gold atoms and 265 nm resonance photolysis into the Au (^2P) state[22] give the same $(H_2)AuH$ and AuH_2 absorptions. Excited gold reacts substantially faster with H_2 than D_2 in the same solid sample. The AuH_2 molecule is trapped owing to the greater stability of the AuH bond compared to AgH and CuH.[5] A small yield of CuH_2 was observed in solid hydrogen, but no evidence was found for AgH_2.

The MH molecules also react further with another metal to synthesize cluster hydrides M_2H. These molecules electron capture to form stable M_2H^- anions.

The vibrational assignments and molecular identifications are confirmed by BPW91 and B3LYP energy, structure, and vibrational frequency calculations using the SDD metal pseudopotentials. The accuracy of these isotopic frequency calculations for coinage metal hydride molecules is significant.

Acknowledgment. We gratefully acknowledge support for this work from NSF Grant CHE 00-78836, results on $NaAu_2H_{1-x}$

compounds from W. Bronger, and assistance of D. Carrére and D. Danset with thermal gold experiments.

References and Notes

(1) (a) Fitzsimons, N. P.; Jones, W.; Herley, P. J. *J. Chem. Soc., Faraday Trans.* **1995**, *91*, 713. (b) Jaschek, C.; Jaschek, M. *The Behavior of Chemical Elements in Stars*; Cambridge University Press: Cambridge, U.K., 1995.

(2) (a) Ram, R. S.; Bernath, P. F.; Brault, J. W. *J. Mol. Spectrosc.* **1985**, *113*, 269. (b) Seto, J. Y.; Morbi, Z.; Charron, F.; Lee, S. K.; Bernath P. F.; Le Roy, R. J. *J. Chem. Phys.* **1999**, *110*, 11756 and references therin.

(3) (a) Gruen, D. M.; Wright, R. B.; Bates, J. K. *Inorg. Chem.* **1978**, *17*, 2275. (b) Ozin, G. A.; Gracie, C. *J. Phys. Chem.* **1984**, *88*, 643. (c) Ozin, G. A.; Mitchell, S. A.; Garcia Prieto, J. *Angew. Chem., Int. Ed. Engl.* **1982**, *21*, 380.

(4) Bengtsson, E.; Olsson, E. *Z. Phys.* **1931**, *72*, 163.

(5) Huber, K. P.; Herzberg, G. *Molecular Spectra and Molecular Structure, Vol. IV, Constants of Diatomic Molecules*; Van Nostrand Reinhold: New York, 1979.

(6) (a) Gerö, A.; Schmid, K. *Z. Phys.* **1943**, *121*, 459. (b) Birk, H.; Jones, H. *Chem. Phys. Lett.* **1989**, *161*, 27. (c) Witek, H. A.; Fedorov, D. G.; Hirao, K.; Viel, A.; Widmark, P. O. *J. Chem. Phys.* **2002**, *116*, 8396.

(7) (a) Wang, X.; Andrews, L. *J. Am. Chem. Soc.* **2001**, *123*, 12899. (b) Wang, X.; Andrews, L. *J. Phys. Chem. A* **2002**, *106*, 3744 (Au + H_2).

(8) (a) Marian, C. M. *J. Chem. Phys.* **1991**, *94*, 5594. (b) Collins, C. L.; Dyall, K. G, Schaefer, H. F.; III *J. Chem. Phys.* **1995**, *102*, 2024. (c) Witek, H. A.; Nakijima, T.; Hirao, K. *J. Chem. Phys.* **2000**, *113*, 8015. (d) Avramopoulos, A.; Ingamells, V. E.; Papadopoulos, M. G.; Sadlej, A. J. *J. Chem. Phys.* **2001**, *114*, 198. (e) Legge, F. S.; Nyberg, G. L.; Peel, J. B. *J. Phys. Chem. A* **2001**, *105*, 7905.

(9) (a) Burkholder, T. R.; Andrews, L. *J. Chem. Phys.* **1991**, *95*, 8697. (b) Hassanzadeh, P.; Andrews, L. *J. Phys. Chem.* **1992**, *96*, 9177. (c) Andrews, L.; Citra, A. *Chem. Rev.* **2002**, *102*, 885.

(10) Frisch, M. J.; Trucks, G. W.; Schlegel, H. B.; Scuseria, G. E.; Robb, M. A.; Cheeseman, J. R.; Zakrzewski, V. G.; Montgomery, J. A., Jr.; Stratmann, R. E.; Burant, J. C.; Dapprich, S.; Millam, J. M.; Daniels, A. D.; Kudin, K. N.; Strain, M. C.; Farkas, O.; Tomasi, J.; Barone, V.; Cossi, M.; Cammi, R.; Mennucci, B.; Pomelli, C.; Adamo, C.; Clifford, S.; Ochterski, J.; Petersson, G. A.; Ayala, P. Y.; Cui, Q.; Morokuma, K.; Malick, D. K.; Rabuck, A. D.; Raghavachari, K.; Foresman, J. B.; Cioslowski, J.; Ortiz, J. V.; Stefanov, B. B.; Liu, G.; Liashenko, A.; Piskorz, P.; Komaromi, I.; Gomperts, R.; Martin, R. L.; Fox, D. J.; Keith, T.; Al-Laham, M. A.; Peng, C. Y.; Nanayakkara, A.; Gonzalez, C.; Challacombe, M.; Gill, P. M. W.; Johnson, B.; Chen, W.; Wong, M. W.; Andres, J. L.; Gonzalez, C.; Head-Gordon, M.; Replogle, E. S.; Pople, J. A. *Gaussian 98*, Revision A.6; Gaussian, Inc.: Pittsburgh, PA, 1998.

(11) (a) Krishnan, R.; Binkley, J. S.; Seeger, R.; Pople, J. A. *J. Chem. Phys.* **1980**, *72*, 650. (b) Frisch, M. J.; Pople, J. A.; Binkley, J. S. *J. Chem. Phys.* **1984**, *80*, 3265. (c) Andrae, D.; Haussermann, U.; Dolg, M.; Stoll, H.; Preuss, H. *Theor. Chim. Acta* **1990**, *77*, 123. (d) Wadt, W. R.; Hay, P. J. *J. Chem. Phys.* **1985**, *82*, 284.

(12) (a) Becke, A. D. *Phys. Rev. A* **1988**, *38*, 3098. (b) Perdew, J. P.; Wang, Y. *Phys. Rev. B.* **1992**, *45*, 13244.

(13) (a) Becke, A. D. *J. Chem. Phys.* **1993**, *98*, 5648. (b) Lee, C.; Yang, W.; Parr, R. G. *Phys. Rev. B* **1988**, *37*, 785.

(14) (a) Milligan, D. E.; Jacox, M. E. *J. Mol. Spectrosc.* **1973**, *46*, 460. (b) Wight, C. A.; Ault, B. S.; Andrews, L. *J. Chem. Phys.* **1976**, *65*, 1244.

(15) Wang, X.; Andrews, L. *J. Am. Chem. Soc.* **2003**, in press.

(16) Kaufman, J. W.; Hauge, R. H.; Margrave, J. L. *J. Phys. Chem.* **1985**, *89*, 3541.

(17) Tremblay, B.; Manceron, L. *Chem. Phys.* **1999**, *250*, 187.

(18) Goubet, M.; Asselin, P.; Manceron, L.; Soulard, P.; Perchard, J.-P. *Phys. Chem. Chem. Phys.* **2003**, in press.

(19) Guo, R.; Balasubramanian, K.;Wang, X.; Andrews, L. *J. Chem. Phys.* **2002**, *117*, 1614.

(20) (a) Garcia-Prieto, J.; Ruiz, M. E.; Novaro, O. *J. Am. Chem. Soc.* **1985**, *107*, 5635. (b) Balasubramanian, K.; Liao, M. Z. *J. Phys. Chem.* **1988**, *92*, 361. (c) Balasubramanian, K.; Liao, M. Z. *J. Phys. Chem.* **1989**, *93*, 89. (d) Balasubramanian, K. *J. Phys. Chem.* **1989**, *93*, 6585.

(21) Manard, M. J.; Bushnell, J. E.; Bernstein, S. L.; Bowers, M. T. *J. Phys. Chem. A* **2002**, *106*, 10027.

(22) Gruen, D. M.; Bates, J. K. *Inorg. Chem.* **1977**, *16*, 2450.

(23) (a) Pyykkö, P. *Chem. Rev.* **1988**, *88*, 563. (b) Schwerdtfeger, P.; Schwarz, W. H. E.; Bowmaker, G. A.; Boyd, P. D. W. *J. Chem. Phys.* **1989**, *91*, 1762. (c) Schwerdtfeger, P.; Boyd, P. D. W.; Burrell, A. K.; Robinson, W. T.; Taylor, M. J. *Inorg. Chem.* **1990**, *29*, 3593.

(24) (a) Andrews, L.; Wang, X.; Alikhani, M. E.; Manceron, L. *J. Phys. Chem.* A **2001**, *105*, 3052 (Pd + H_2). (b) Andrews, L.; Wang, X.; Manceron, L. *J. Chem. Phys.* **2001**, *114*, 1559 (Pt + H_2).

(25) Hauge, R. H.; Kafafi, Z. H.; Magrave, J. L. In *Physics and Chemistry of Small Clusters*; Jena, P., Rao, B. K., Khanna, S. N., Eds.; Plenum Press: 1987; Vol. 158, p 787.

(26) Hotop, H.; Lineberger, W. C. *J. Phys. Chem. Ref. Data* **1985**, *14*, 731.

(27) Bronger, W. Personal communication, 2003.

(28) Kang, H.; Beauchamp, J. L. *J. Phys. Chem.* **1985**, *89*, 3364.

(29) Reaction energies calculated at the BPW91 level.

(30) Moore, C. E. *Atomic Energy Levels, Vol. II*; National Bureau of Standards: Washington, DC, 1952.

(31) Greene, T. M.; Brown, W.; Andrews, L.; Downs, A. J.; Chertihin, G. V.; Runeberg, N.; Pyykkö, P. *J. Phys. Chem.* **1995**, *99*, 7925.

(32) Wang, X.; Andrews, L. *J. Am. Chem. Soc.* **2003**, *125*, 6581.

(33) Kroes, G.-J. *Prog. Surf. Sci.* **1999**, *60*, 1 and references therein.